Newly discovered active faults in the Wairarapa Valley: Implications for multi-fault rupture and kinematics in the southern North Island, Aotearoa New Zealand

G. L. Coffey[a]*, N. J. Litchfield[b], R. Morgenstern[b], R. M. Langridge[b], D. Townsend[b]

[a]*Earth Structure and Processes, GNS Science, Dunedin, New Zealand;* [b]*Earth Structure and Processes, GNS Science, Lower Hutt, New Zealand*

* g.coffey@gns.cri.nz

This preprint was submitted to the New Zealand Journal of Geology and Geophysics (NZJGG), has undergone peer review, and is now accepted. It will be published open access. Due the migration of NZJGG over to Wiley there are delays in publication and a DOI is not expected until January/February of 2026.

Newly discovered active faults in the Wairarapa Valley: Implications for multi-fault rupture and kinematics in the southern North Island, Aotearoa New Zealand

G. L. Coffey[a]*, N. J. Litchfield[b], R. Morgenstern[b], R. M. Langridge[b], D. Townsend[b]

[a]Earth Structure and Processes, GNS Science, Dunedin, New Zealand; [b]Earth Structure and Processes, GNS Science, Lower Hutt, New Zealand

* g.coffey@gns.cri.nz

Newly discovered active faults in the Wairarapa Valley: Implications for multi-fault rupture and kinematics in the southern North Island, Aotearoa New Zealand

Abstract

Active fault locations and constraints on the timing and size of earthquakes are important for understanding and mitigating seismic hazard in Aotearoa New Zealand. However, historical and instrumental records are too short to provide these data on most earthquake-generating faults. Light detection and ranging (lidar) data provide us with the ability to locate and describe active faults and importantly, help us fill gaps in the paleoseismic record. A recent update to active fault mapping in the Wairarapa Valley has led to the discovery of seven new faults along with many new traces along previously identified faults. Four of these newly identified faults, (the Ruamahanga, Woodside, Carters Line, and Pāpāwai faults) are close to population centres and have slip rates and recurrence intervals of 0.1 - 1.1 mm/yr, and 770 - <15,000 years respectively. This work has revealed that active faults are distributed more widely across the Wairarapa Valley than previously thought, particularly in areas of geometric complexity. Fault-scarp gradients and paleoseismic constraints developed here suggest that faults in the Wairarapa Valley tend to rupture as part of multi-fault earthquakes with surface rupture during the 1855 CE earthquake on the Wairarapa Fault being more widespread than previously thought.

Introduction

Straddling the boundary between the Pacific and Australian plates, Aotearoa New Zealand (A-NZ) (Figure 1A) is home to nearly 900 mapped active faults, which help to

accommodate oblique convergence across the plate boundary (Seebeck et al., 2024). Mitigating the hazard posed by earthquakes on these active faults requires knowledge of their location as well as constraints on the frequency and size of earthquakes that they may generate, particularly in and around urban centres and important infrastructure. Furthermore, it is becoming increasingly clear that multi-fault ruptures are more common in A-NZ than previously thought, with a number of historical earthquakes identified as multi-fault events (Beanland et al., 1989; Hamling et al., 2017; Holdgate & Grapes, 2014; Nicol et al., 2022; Schermer et al., 2004). Understanding the prevalence, or not, of such events has implications to how seismic hazard is assessed and modelled across the country.

Active fault locations and their paleoseismic data provide geological constraints on the location, timing, and size of past (and future) large to great earthquakes when applied in seismic hazard models (Coffey et al., 2023; Gerstenberger, Bora, et al., 2024; Litchfield et al., 2023; Seebeck et al., 2023; Stirling et al., 2012). Additionally, these data inform databases that guide regional planning and policy decisions, for example the New Zealand Active Faults Database (NZAFD) and the Quarter Million Map (QMAP) of New Zealand (Heron, 2023; Langridge et al., 2016; Morgenstern et al., 2024). Consequently, our ability to understand earthquake behaviour across A-NZ and mitigate the hazard posed by future earthquakes depends on the quality and completeness of active fault databases that underpin regional and nationwide models.

Typically, active faults are mapped based upon their expression in the landscape, as indicated by the presence of ground deformation such as a vertical offset or fault scarp. Desktop investigation of such ground deformation is achieved through interrogation of elevation and surface datasets of varying resolution. These commonly include aerial photography and satellite imagery, as well as other remote sensing datasets such as light

detection and ranging (lidar) digital elevation models and photogrammetry-derived digital surface models. Lidar can provide a high-resolution, bare-Earth model of the ground surface with finer than 1-m pixel resolution, which makes the detailed identification of even subtle ground-surface fault traces possible. With steadily increasing lidar coverage across A-NZ many previously undiscovered active faults have been identified and mapped, at an average rate of seven per year since 2010, and existing faults have been characterised in greater detail. It is worth noting though, that even with an increase in lidar acquisition, geomorphic evidence for past earthquakes is removed from the landscape over time through weathering and erosion. As a result, some mapped faults have only been discovered because they ruptured historically (e.g. Greendale, White Creek; Berryman 1980; Quigley et al. 2010) and many unmapped or unknown faults have been postulated across A-NZ (Nicol, Van Dissen, et al., 2016). Continuing to update active fault maps across the country will improve our understanding of the spatial distribution of active faults and how strain is accommodated (and released) across the A-NZ plate boundary.

The southern North Island of A-NZ is home to 10% of A-NZ's population (Stats NZ accessed January 2025, https://tools.summaries.stats.govt.nz/) and is traversed by numerous north to northeast striking faults that accommodate both dextral strike-slip and reverse slip (Figure 1B). Lidar acquisition across the southern North Island coupled with the need to update active fault data for a revision of the Combined Wairarapa District Plan provided an opportunity to re-evaluate active fault mapping across the Southern Wairarapa, Carterton, and Masterton districts at a scale of less than 1:10,000 (Litchfield et al., 2022). The Litchfield et al. (2022) study led to the identification of many new surface traces along previously mapped faults as well as the discovery of seven previously unidentified active faults. A follow-up study provided ground truthing and preliminary

slip rate data for four of the newly identified active faults, the Pāpāwai, Ruamahanga, Carters Line, and Woodside faults (Figure 2) (Coffey & Litchfield, 2023). In this paper we summarise key results from Litchfield et al. (2022) and Coffey & Litchfield (2023) and build on these reports to use the new mapping and measurements of scarp gradient to explore the potential of multi-fault rupture in A-NZ. We also discuss fault kinematics across the Wairarapa Valley and potential changes to future versions of fault models such as the New Zealand Community Fault Model (CFM) (Seebeck et al., 2024).

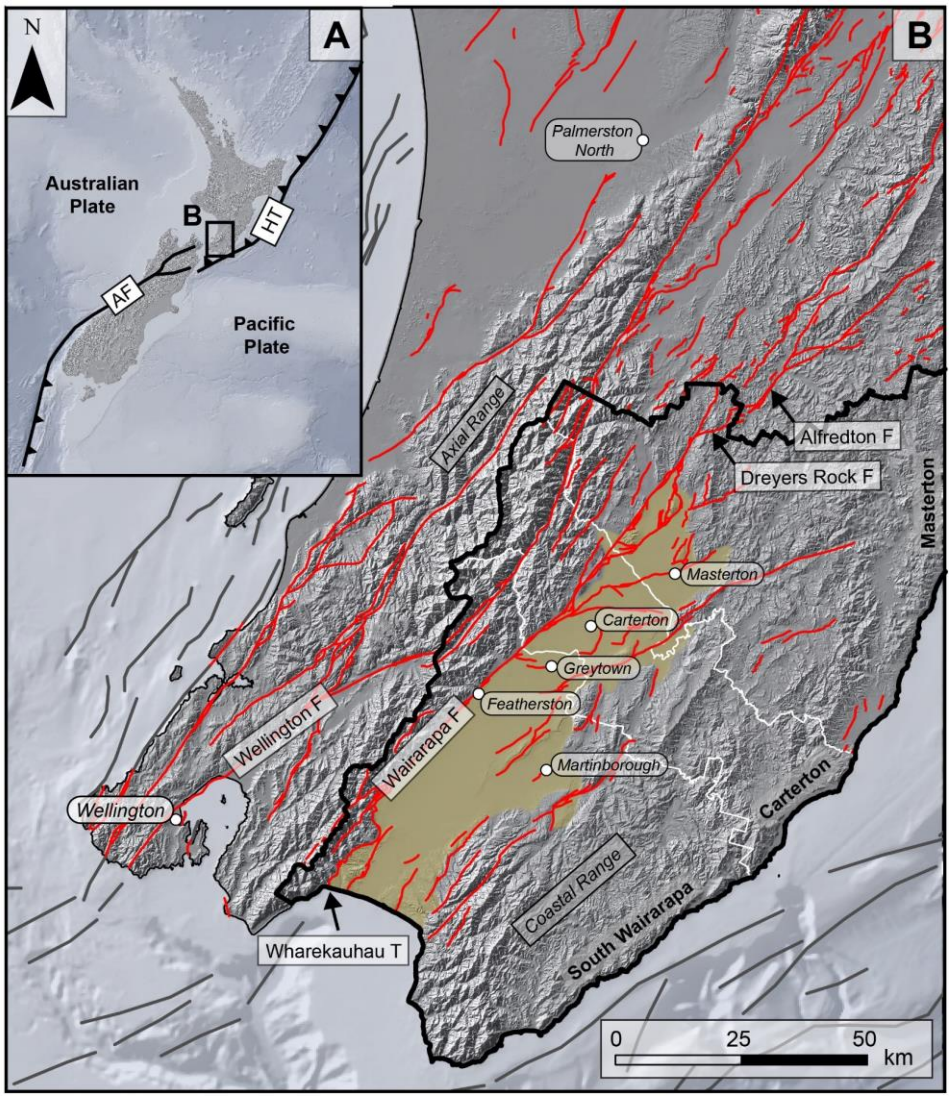

Figure 1 – Tectonic overview of A) the Aotearoa - New Zealand plate boundary and B) the southern North Island. AF is the Alpine Fault and HT is the Hikurangi Trough. Onshore active faults are shown in red and are from the 1:250,000 scale New Zealand Active Faults Database (Langridge et al. 2016) and includes updated active fault mapping presented in this paper. Offshore faults are shown in dark grey (Barnes et al., 2010; Nodder et al., 2007). The Wairarapa Valley is shaded in yellow. The Wairarapa Region is indicated by the bold black outline and district boundaries (South Wairarapa, Carterton, Masterton) are indicated by the white lines.

Tectonic and geologic setting

Across the southern North Island the Pacific Plate is obliquely converging with the Australian Plate at a rate of ~40 mm/yr (Beavan et al., 2002; Darby & Beavan, 2001; DeMets et al., 1990). Most of the contractional motion is accommodated by subduction of the Pacific Plate beneath the Australian Plate at the Hikurangi Trough (Figure 1A) (Nicol & Beavan, 2003; Wallace et al., 2004). However, a component of convergence has also been transferred to the overriding plate, where structural observations such as growth strata and unconformities indicate variable rates of shortening over time (Cape et al., 1990; Lamb & Vella, 1987; Nicol & Beavan, 2003). A belt of predominantly dextral strike-slip faults extends onshore from the south coast of Wellington and along the Axial Range to form the North Island Fault System (NIFS). The NIFS, which includes the Wellington and Wairarapa faults, accommodates up to 22 mm/yr of plate-boundary parallel motion along with a minor component of convergence (Carne et al., 2011; Nicol & Wallace, 2007; Ninis et al., 2022). In the east, the Coastal Range is the surface expression of the inner, uplifted, part of the Hikurangi subduction wedge and hosts numerous reverse bedrock faults, which are mostly thought to be inactive (Bailleul et al., 2007; Begg & Johnston, 2000; Lee & Begg, 2002; Neef, 1995). Sandwiched between the Axial and Coastal ranges is the low-lying Wairarapa Valley (Figure 1B), which is a remnant fore-arc basin that is crossed by several active faults branching off the Wairarapa Fault, including the Masterton, Carterton, and Mokonui faults (Beanland et al., 1998; Townsend et al., 2002; Zachariesen et al., 2000) (Figure 1, Figure 2).

The geology of the Wairarapa Region is mostly comprised of Pleistocene and younger sediments that blanket most of the Wairarapa Valley and older bedrock in the Axial and Coastal ranges (Figure 2). The surrounding bedrock predominantly comprises Torlesse Terrane sandstones, greywackes and argillites in the Axial Range, and Pliocene

– Miocene age limestone, mudstones, and sandstones in the Coastal Range (Figure 2) (Begg & Johnston, 2000; Lee & Begg, 2002). The Pleistocene-Holocene sediments are mainly alluvium from aggradation of large, braided rivers flowing from the Axial and Coastal ranges during the cold glacial or interstadials (Vella 1963; Palmer et al. 1989; Litchfield and Berryman 2005) with some lake deposits, primarily from the last interglacial and Holocene (Warnes 1992). The gravel dominated Pleistocene-Holocene sediments form broad terraces, summarised in Table 1, with the most widespread of these being the extensive Last Glacial Maximum Waiohine terrace (Q2al, 12 ± 2 ka) (Vella, 1963; Warnes, 1992). These terraces can be distinguished from each other by their relative height above river level, morphology and loess cover; for example, older terraces are typically smoother and rounded.

Numerous active faults have previously been identified across the Wairarapa Region. These include: the Wellington Fault in the Axial Range, the Carterton, Masterton, and Te Maire faults which crosscut the Wairarapa Valley, and the eastern part of the Carterton Fault in the Coastal Range, which here we refer to as the Eastern Carterton Fault (Langridge et al., 2016) (Figure 1B, Figure 2). The Wairarapa Fault bounds the southeastern side of the Axial Range and splits towards its northern end to form the Dreyers Rock and Alfredton faults (Figure 1B) (Schermer et al., 2004). It is the only fault in the southern North Island known to have ruptured the ground surface since European settlement of A-NZ in the 1855 CE M_w 8.2 Wairarapa Earthquake, where up to 18 m of horizontal displacement occurred on the Wairarapa Fault (Grapes & Downes, 1997; Rodgers & Little, 2006). Paleoseismic investigations have shown that the Wairarapa Fault has a recurrence interval of 1230 ± 190 years (Humphrey et al., 2025; Little et al., 2009) and a slip rate of 12.1 ± 3 mm/yr at its southern end (Carne et al., 2011), which decreases to 6 ± 1 mm/yr towards the north (Seebeck et al., 2023; Van Dissen & Berryman, 1996;

Villamor et al., 2008). Previous work has also proposed, that the 1855 CE Wairarapa earthquake was a multi-fault rupture, which included the onshore Wharekauhau Thrust, Dreyers Rock and Alfredton faults, and possibly the subduction thrust together with the offshore Vernon, Needles and Nicholson Bank faults (Holdgate & Grapes, 2014; Humphrey et al., 2025; Rodgers & Little, 2006; Schermer et al., 2004). While there are numerous other active faults in and around the Wairarapa Valley, these have received comparatively little attention. Offsets have been identified along the Huangarua Fault and lead to slip rates of 0.4 – 0.8 mm/yr (Lamb & Vella, 1987; Nicol et al., 2002). Paleoseismic trenches have been excavated across the Carterton, Mokonui, and Masterton faults, which show that they rupture the ground surface with metre-scale displacements roughly every 2000 – 3500 years (Begg et al., 2001; Langridge et al., 2003; Litchfield et al., 2023; Townsend et al., 2002; Zachariesen et al., 2000).

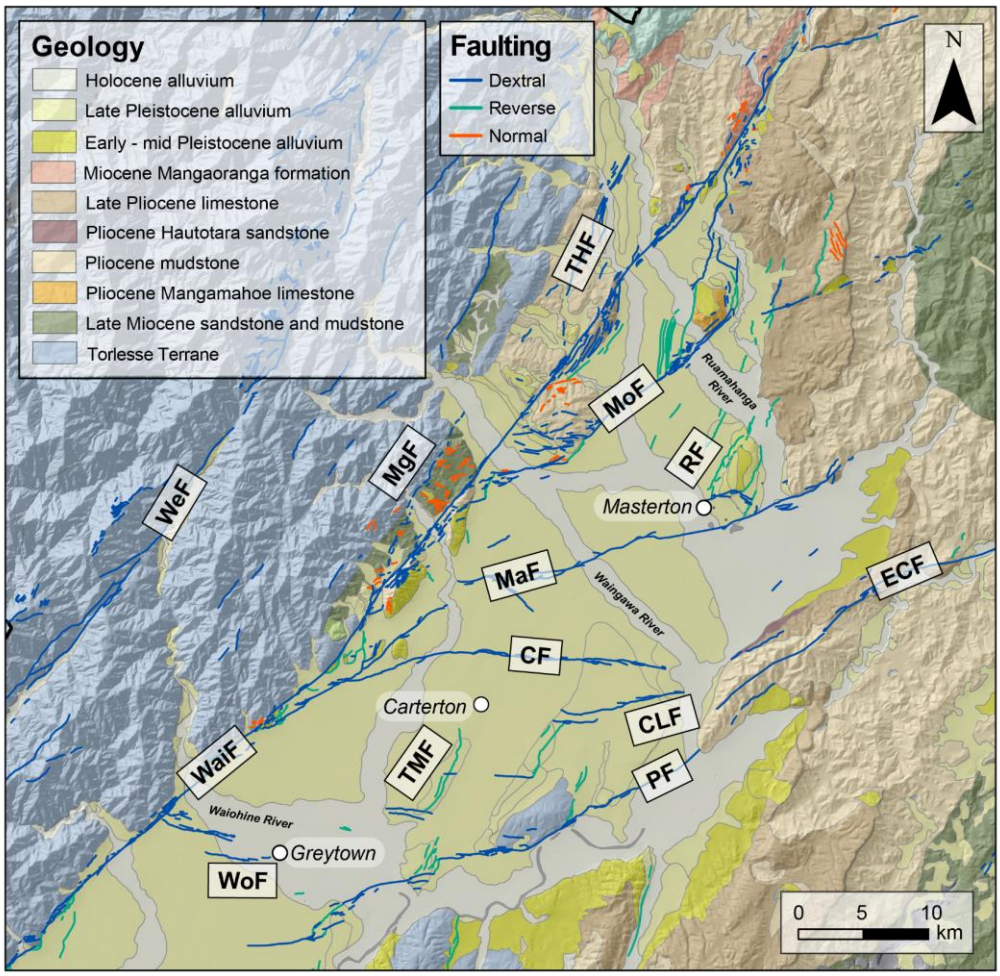

Figure 2 - Geological and faulting overview of the northern Wairarapa Valley. Generalised geological units are from the 1:250,000 Quarter Million Map (QMAP) (Begg & Johnston, 2000; Lee & Begg, 2002). Active fault mapping is coloured by dominant slip sense and includes the newly identified Woodside (WoF), Carters Line (CLF), Pāpāwai (PF), Ruamahanga (RF), Te Hau (THF), and Mangaterere (MGF) faults, as well as updates to the Wellington (WeF), Wairarapa (WaiF), Mokonui (MoF), Masterton (MaF), Carterton (CF) and Eastern Carterton (ECF) faults.

Description of newly mapped active faults

Prior to the Litchfield et al. (2022) study, the total cumulative length of active fault surface traces mapped across the Wairarapa Region was 720 km (Langridge et al., 2016). With the acquisition of lidar data (± 10 – 15 cm one-sigma vertical uncertainty; Supplementary Materials S3) updated active fault mapping has increased the total length of fault traces in the region by ~50% resulting in a total cumulative active fault length of 1100 km (Figure 3). All updates to active fault mapping are summarised in Litchfield et al. (2022) and the updated fault traces are viewable on the GNS Science high-resolution

dataset of the New Zealand Active Faults Database (Morgenstern et al., 2024), Wairarapa Maps Online, and Greater Wellington Maps Viewer (Hazards and Emergency Management). A shapefile of the updated mapping is available upon request.

Most newly mapped traces are relatively short (< 1 km) and accommodate reverse and/or dextral slip (Figure 2). Due to the additional mapped fault traces, geometric complexity has been added to previously identified faults. This includes more distributed deformation along the Wellington, Wairarapa, and Mokonui faults, splaying of the Masterton Fault off the Carterton Fault instead of the Wairarapa Fault, and increased surface deformation associated with fault intersections and changes in fault strike (Figure 3). Seven previously unrecognised faults were identified: the Ruamahanga, Carters Line, Pāpāwai, Woodside, Te Hau, Wharekauhau East, and Mangaterere faults (Figure 3). The Te Hau and Mangaterere faults are relatively short (both with lengths of ~12 km), north-northeast-oriented faults that extend along the eastern foothills of the Axial Range. The Wharekauhau East Fault is in the southwestern corner of the Wairarapa Valley (Figure 3). It is a short (~7 km-long), northeast-oriented reverse fault that is located south and along strike of the Battery Hill Fault (Figure 3) but with an opposite sense of throw of down-to-the-southeast. The four remaining faults: the Pāpāwai, Carters Line, Ruamahanga, and Woodside faults cut across the northern Wairarapa Valley and are described in more detail below. The Mokonui Fault is also described in detail here due to the discovery of many new traces along its length and consequently, a considerable increase in its complexity. In addition to the discovery of fault traces, re-evaluation of fault mapping has also led to the removal of the Ngāpotiki Fault (Figure 3A). The Ngāpotiki Fault previously was mapped to extend through the southeastern Coastal Range (Begg & Johnston, 2000), however very few scarps could be identified in the lidar data and we therefore consider this fault to be inactive. We emphasise that the mapping

summarised here was focused on areas within the Wairarapa Valley, particularly around townships, as well is in areas around previously identified major faults, for example the Wellington and Wairarapa faults. Consequently, mapping may be incomplete in parts of the Axial and Coastal ranges. However, evidence for surface faulting is much less common through these ranges, which may in part be due to steep slopes and rapid erosion of the Cenozoic mudstones here (Lee & Begg, 2002), and it is likely that only minor faulting that is absent.

In addition to updating active fault mapping, terrace mapping was also revisited as alluvial terraces provide age control for the timing of offset. Updated terrace mapping was focused near faults in the northern Wairarapa Valley and incorporates results from previous studies as well as updates based on the interpretation of lidar data. The results of terrace mapping are presented in Table 1 and Figure 4. Terrace mapping was undertaken in the immediate vicinity of faults in the northern Wairarapa Valley to refine terrace boundaries and account for any reinterpretations that result from updated fault mapping. The main consequences of this remapping were: (1) subdivision of the Q1al terraces (i.e the youngest terraces) in areas proximal to faults, (2) addition of a Q5al terrace at site A (Figure 4), (3) addition of a Q4al terrace at site B (Figure 4), (4) addition of a possible Q3al terrace at site C (Figure 4), and (5) refinements of the Q8al, Q6al and Q4al terraces at site D (Figure 4) based on reinterpretation of the surface morphology.

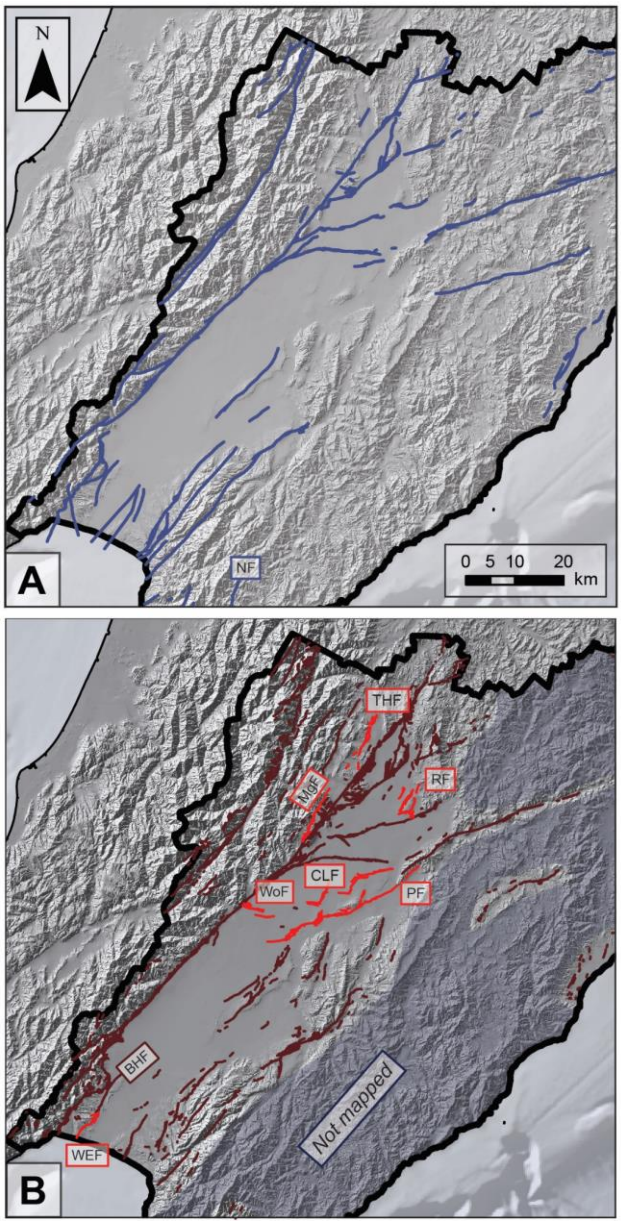

Figure 3 - Active faults mapped in the Wairarapa Region prior to (A) and after (B) the lidar mapping described in this work. Previous mapping shown in (A) is from the 1:250,000 scale New Zealand Active Faults Database (NZAFD; Langridge et al. 2016; Morgenstern et al. 2024). Faults shown in (B) includes the updated mapped active fault traces, which are coloured maroon if they had previously been identified and in red if they were newly identified as part of this work. Newly identified faults are as follows: Wharekauhau East (WEF), Woodside (WoF), Pāpāwai (PF), Carters Line (CLF), Mangaterere (MgF), Ruamahanga (RF), and Te Hau (THF) faults. One fault was removed upon re-evaluation of fault mapping, the Ngāpotiki Fault (NF). The Battery Hill Fault (BHF) is also indicated. The blue shaded polygon in (B) encompasses the areas within the Coastal Range where mapping was not focused. All updated active fault mapping can be found on the NZAFD (https://data.gns.cri.nz/af/).

Table 1 – summary of alluvial terraces mapped across the Wairarapa Valley and their ages

Terrace Name	Age of Formation (ka)	Age of Abandonment (ka)	References*
Q1al	<10	< 10	Formento-Trigilio et al. (2002); Tompkins (1987)

Q2al (Waiohine terrace)	18–10	12 ± 2	Carne et al. (2011); Formento-Trigilio et al. (2002); Litchfield and Berryman (2005); Tompkins (1987); Wang and Grapes (2008)
Q3al	50–31	35 ± 4	Formento-Trigilio et al. (2002); Litchfield and Berryman (2005)
Q4al	70–50	55 ± 5	Formento-Trigilio et al. (2002); Litchfield and Berryman (2005)
Q5al	130–90	90 ± 5	Palmer et al. (1989); Warnes (1992)
Q6al	160–140	140 ± 5	Litchfield and Berryman (2005)

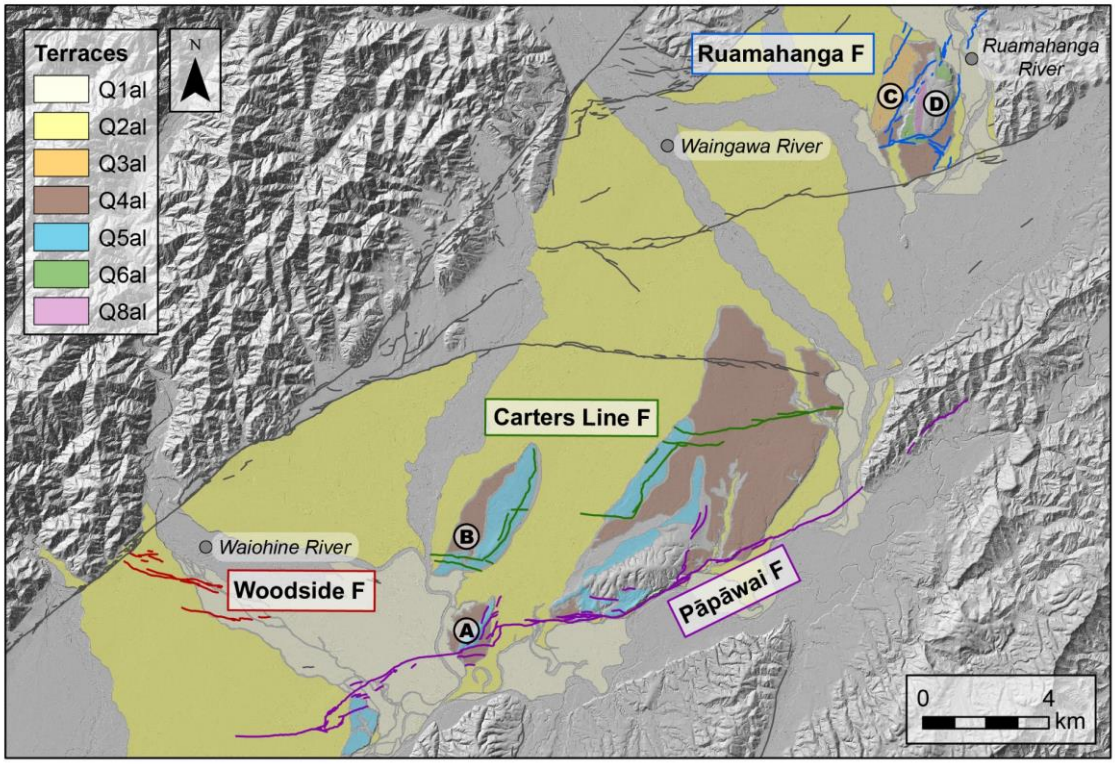

Figure 4 - Revised terrace mapping in the northern Wairarapa Valley. The Ruamahanga, Carters Line, Woodside, and Pāpāwai faults are indicated by the coloured lines. All other faults are shown in dark grey. Circled letters indicate the main sites where terrace mapping changed and are discussed in the text.

Ruamahanga Fault

The most northern of the faults discovered, the Ruamahanga Fault, branches off the Masterton Fault at a high angle and extends north-northeast for a total length of ~6 km (Figure 2, Figure 5B). It consists of a set of predominantly reverse, west side up, northeast-southwest striking traces and a set of < 1 km long east-west oriented dextral-strike slip traces, most of which had previously been mapped but considered part of the

Masterton Fault. Traces broadly bound either side of an uplifted block of Q4al-Q8al terraces before extending across younger Q1al surfaces further north (Figure 4) (Lee & Begg, 2002). Where the fault crosses these younger surfaces towards the north, its surface expression becomes scalloped, possibly indicating a transition to shallower angle thrust faulting.

Woodside Fault

The Woodside Fault extends from the Wairarapa Fault about 10 km west of Greytown as a series of ~100 m- to 4 km-long east-southeast trending traces across Q1al and Q2al surfaces, into the outskirts of Greytown (Figure 2, Figure 5C). No scarps were identified in Greytown, however the possibility that the fault may be concealed beneath these young terraces and the active riverbed of the Waiohine River cannot be excluded. The Woodside Fault appears to be mainly dextral strike-slip with a minor component of vertical slip (down to the north-northeast and down to the south-southwest; Figure 5C). Close to the Wairarapa Fault the Woodside Fault has a sharper and higher scarp (up to 1.9 m in height) and horizontally offset terrace risers have been identified along its length (Supplementary Figure S3). Elsewhere, the Woodside Fault crosses a younger surface, and its vertical expression is subtle, with scarp heights of only up to 40 cm.

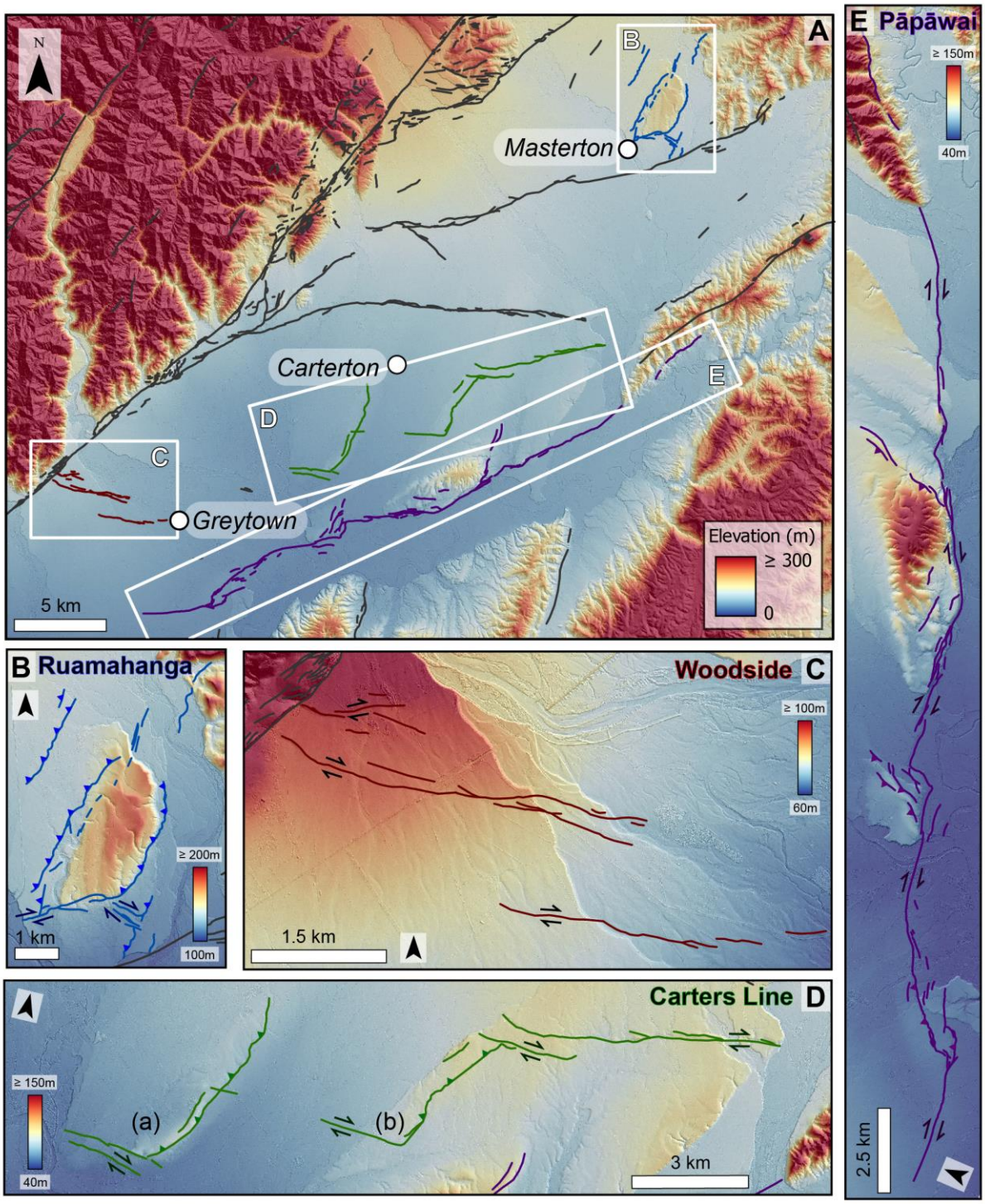

Figure 5 – The four newly mapped active faults in the northern Wairarapa Valley that are described in the text. A) Location and overview of the four faults discussed in the text. The Ruamahanga Fault is shown in blue, the Woodside Fault in yellow, the Carters Line Fault in green and the Pāpāwai Fault in purple. B – E) Detailed mapping for each fault. (a) and (b) in panel D are grouped traces of the Carters Line Fault discussed in the text. Note the orientation of the north arrow and colour scale changes between panels.

Carters Line Fault

The Carters Line Fault has been mapped south and east of Carterton and consists of two distinct L-shaped groups of traces (Figure 2, Figure 5D). Here, we refer to these

as groups (a) and (b) for the western and eastern set, respectively. These groups each contain a subset of east-west striking traces, which host predominantly dextral strike-slip motion, as well as a subset of northeast-southwest striking traces that are predominantly reverse in sense. Several of the east-west traces are subparallel to the Woodside Fault and the western Carterton Fault and although the distance between the Woodside and Carters Line faults is ~7.5 km and considered a real gap, we discuss the implications of the potential linkage between these faults with respect to the New Zealand CFM in the Discussion section. The highest scarps occur along northeast-southwest-striking traces within group (a), which cross a high Q5al surface (Figure 4). These scarps are up to 18 m in height and are generally broad, with vertical deformation occurring over across-strike widths of ~50 m. Fault traces within group (b) are more subtle, predominantly dextral strike slip and have scarps up to 5 m in height across a Q5al surface (Figure 4). Traces of the Carters Line Fault, along with traces of the Carterton and Pāpāwai faults, all appear to converge eastwards towards the Eastern Carterton Fault where it traverses the Coastal Range (Figure 2, Figure 5A).

Pāpāwai Fault

Southeast of the Carters Line and Woodside faults is the Pāpāwai Fault, the longest of the newly identified faults, with an overall length of ~26 km (Figure 5E). It forms a mostly continuous fault trace which extends from south of Greytown to the Ruamahanga River along-strike from the eastern part of the Carterton Fault (Figure 2, Figure 5A). The overall strike is northeast, subparallel to the eastern Carterton Fault but more northerly than the western Carterton Fault, highlighting the possibility that the Pāpāwai Fault and the eastern part of the Carterton Fault are parts of the same structure. We examine this further in the Discussion section. Towards its centre it bounds the southeast side of a lozenge-shaped block of hills exposing Torlesse Terrane bedrock,

while a strand splaying off the main trace bounds the eastern side of this block, continuing for 3.5 km to the north-northeast (Figure 5E). Similar to the Carters Line Fault, the Pāpāwai Fault consists of a mix of east-west and northeast-southwest striking faults, which host predominantly dextral strike-slip and reverse slip motion (mostly up to the northwest), respectively. Along most of its length, the Pāpāwai Fault has one main trace, however there are pockets of more distributed faulting. Traces within these pockets are typically between 100 m and 1.4 km in length and occur mainly in areas where there is a change in fault strike.

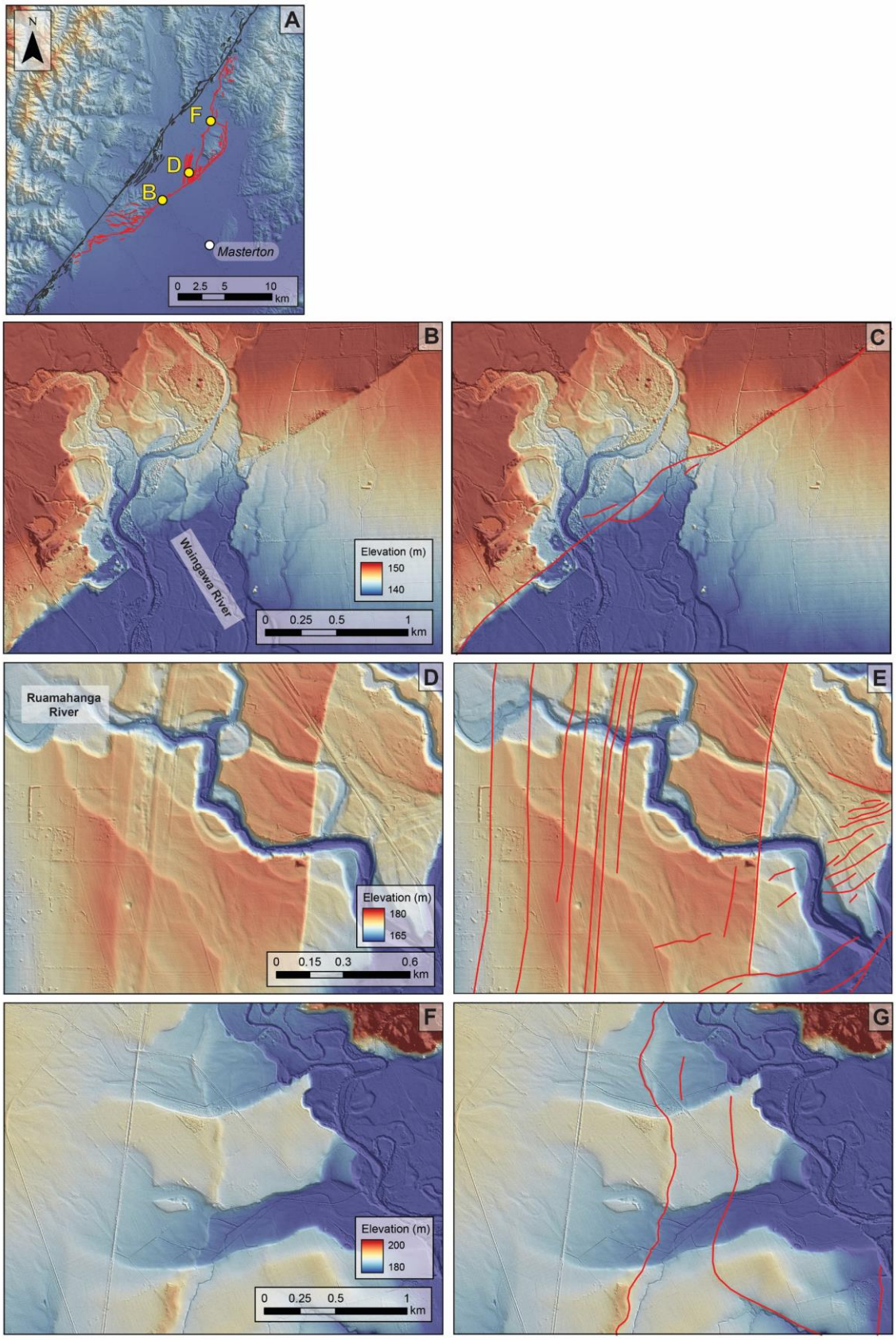

317

318 *Figure 6 – Examples of mapping of the Mokonui Fault from lidar data. A) Overview of the Mokonui Fault (red) and*
319 *the northern Wairarapa Fault (dark grey). B, D, and F) Lidar maps demonstrate kinematic styles of the Mokonui Fault.*
320 *C, E, G) Annotated versions of B, D, and F) with the Mokonui Fault shown in red.*

Mokonui Fault

The new lidar mapping of the Mokonui Fault confirmed some traces that were previously mapped as 'possible' faults (Townsend et al. 2002), showing that it connects to the Wairarapa Fault at both ends (Figure 6A). Along much of its length, it is defined by a single sharp, relatively continuous, down-to-the-southeast, northeast-southwest striking scarp (Figure 6B, C); however, there are some locations where its surface expression is more distributed. Distributed deformation is observed on the northeast side of the Waingawa River (Figure 2), where numerous short east-west striking traces link the Mokonui Fault to the Wairarapa Fault (Figure 6A). Distributed deformation is also observed on the southwest side of the Ruamahanga River (Figure 2) where the Mokonui Fault branches into multiple traces and swings in strike ~60° counterclockwise to become north-south striking and bound either side of a bedrock-cored block (Figure 2). The western of these traces are a series of remarkably sharp, straight, parallel, very closely spaced (20 – 200 m apart), north-south striking traces that range from 700 m to 2.5 km long(Figure 6D, E). These 'train-track'-like scarps crosscut and vertically offset fluvial channels by up to ~4 m with no clear horizontal offset. It is possible that these are bedding-plane faults, exploiting pre-existing planes of weakness in the bedrock, however the lack of bedrock exposure here prevents validation of this hypothesis. North of the limestone block (Pliocene Mangamahoe limestone in Figure 2), the Mokonui Fault continues north across a Q3al surface and its expression changes once more. Here the Mokonui Fault scarp has a sinuous morphology (Figure 6F, G) which we interpret to be the result of a shallowing of fault dip, relief on the terrace surface (e.g. channelisation), and/or smaller-scale variations in its fault plane geometry.

Methods of paleoseismic characterisation of the Ruamahanga, Woodside, Carters Line, and Pāpāwai faults

Desktop geomorphic analysis, described below, was used to provide some constraint on slip rate, (SED), magnitude and mean recurrence interval for the Ruamahanga, Woodside, Carters Line, and Pāpāwai faults. As estimates of these parameters come from lidar data and scaling relationships based upon simplified full-fault rupture, constraints are first order. Further work such as paleoseismic trenching should be undertaken to validate these paleoseismic constraints and reduce the uncertainties. Semi-automated analysis of fault scarp gradients across the northern Wairarapa Valley was also completed to provide a quantitative measure of fault sharpness across a broad area. Scarp slope has been shown to be inversely correlated to time elapsed since the last earthquake (Hodge et al., 2019; Middleton et al., 2016). We systematically measured scarp gradients at regular intervals along faults and take scarp gradient as a proxy for time since the last event to identify faults that may have experienced, for example, a historical surface-rupturing earthquake such as the 1855 CE Wairarapa Earthquake.

Slip rate, recurrence interval, and single event displacement

Vertical displacements were measured using fault scarp heights to place bounds on vertical slip rate. Fault-perpendicular topographic profiles were constructed along each of the four faults where a clear scarp could be identified in the lidar, following the method defined by Howell et al. (2020) (Figure S2). Each vertical offset measurement is assigned a quality factor (QF) of 1 – 3, where 3 is excellent (clearly offset surface where hanging wall and footwall gradient can be confidently defined) and 1 is poor (hanging wall and footwall surface gradients cannot be defined). Vertical offset measurements from the same fault strand and surface were grouped together and those that had a QF $\geq$ 2 were used to calculate an average vertical offset. Only those average vertical offsets that were

calculated from at least three QF ≥ 2 quality measurements were used to calculate vertical slip rate. Horizontal offsets were measured using the MATLAB tool LaDiCaoz (Zielke & Arrowsmith, 2012), a lateral displacement calculator that back-slips or reverses an offset geomorphic feature, such as a channel or terrace riser, to its original configuration (Figures S3, S4). A Monte Carlo approach was adopted to calculate horizontal, vertical and net slip rates by sampling Gaussian distributions of surface age, offset, and fault dip. Estimates of surface age are from updated terrace mapping (Figure 4) and QMAP (Begg & Johnston, 2000; Lee & Begg, 2002). Fault dip is used to calculate net slip rates and is assigned based upon nearby similarly oriented faults in the CFM. Sections of faults that are predominantly reverse in sense are assigned dips of 70° ± 10°, while those that are predominantly dextral are given a dip of 80 ± 10° (Seebeck et al. 2024). These dips are estimates and reflect that faults accommodate a combination of reverse and dextral slip. In places where a fault consists of multiple strands, slip rates across the strands are summed. Table 2 presents a summary of the slip rate determinations and further details can be found in Table S1 and S2.

Recurrence intervals and SEDs were calculated using scaling relationships from the 2022 NSHM (Gerstenberger, Bora, et al., 2024; Gerstenberger, Van Dissen, et al., 2024; Stirling et al., 2023). The average SED (D) for each fault is related to rupture length (L) and seismic moment (M_0) by the following:

$$D = \frac{M_0}{L \times Z \times \mu} \quad (1)$$

Z is rupture depth, which is defined by a D90 (the depth above which 90% of the seismicity in a region occurs) of 16 – 19 km from Ellis et al. (2023) and μ is crustal rigidity, assumed to be 3.0×10^{10} Nm^{-2}. The rupture length is assumed to be the overall length of the fault (or group of fault traces); therefore, the resulting constraints correspond

to rupture of a single fault along its entire length. Seismic moment, M_0, is derived from the following:

$$M_0 = 10^{(1.5Mw+9.5)} \quad (2)$$

$$M_w = log_{10}(LZ) + c \quad (3)$$

where M_w is moment magnitude for a simplified full-fault rupture and c is a constant between 4.1 and 4.3. Recurrence interval for each fault was then calculated by dividing the average SED by the net slip rate, which we assume is constant along fault. The resulting SED and RI constraints are summarised in Table 2.. We do not consider multi-fault rupture in these calculations, which would likely increase the resulting magnitude for faults that co-rupture together, although we explore the potential scenario of a Woodside-Carters Line fault rupture to facilitate its inclusion in the CFM in the Discussion section.

Fault scarp gradients

Scarp gradients were calculated from a lidar-derived digital elevation model (with ± 10 – 15 cm one-sigma vertical uncertainty) along the Wairarapa, Carterton, Masterton, Mokonui, Carters Line, Ruamahanga, Pāpāwai, and Woodside faults at 100 m intervals. At each point, elevation data are extracted along a 60 m profile oriented orthogonal to the fault trace and the steepest scarp gradient within a 2 m horizontal interval is identified and the slope angle calculated (Figure 7). This 2 m horizontal interval was chosen to facilitate automated assessment of scarp gradient across fault scarps with varying width, ensuring that footwall and hanging wall ground surfaces were not included in the measurement. Manual and automated checks were made to ensure that 1) the feature being measured is a fault scarp and not another feature such as a terrace riser or man-

made structure, and 2) that the feature being measured does not form the boundary between surfaces of different age. We discarded results from profiles that failed these three checks. We plot maximum gradient against slip style (Supplementary Figure S5) and see no clear correlation with dominantly reverse, dextral, and strike-slip faults all having a similar median gradient. While there is generally an inverse relationship between maximum scarp gradient and time since the last earthquake, we acknowledge that other factors may influence fault scarp gradient such as lithology and fault plane dip (Hodge et al., 2019; Hodge et al., 2020; Papanikolaou et al., 2005). While slip sense may influence scarp gradient through fault dip, the faults analysed here all accommodate a combination of reverse and dextral strike slip motion, which will reduce fault dip related impacts to scarp gradient. To correct for any potential bias in surface age we use an age factor between zero and one to normalise the scrap gradient, where one corresponds to the abandonment age of a Q6al surface and zero corresponds to a Q1al surface. These bounds are chosen as they reflect the range of alluvial surfaces crosscut by active faulting across the northern Wairarapa Valley (Figure 4). The maximum gradient measured at each point was then divided by its corresponding age factor. Doing this allows us to account for differences in the material type (e.g. mudstone in the Q5al surface, thicker loess sequences with increasing surface age) (Palmer et al., 1989; Vella, 1963; Warnes, 1992), as well as to place more weight on sharper traces that cut younger surfaces.

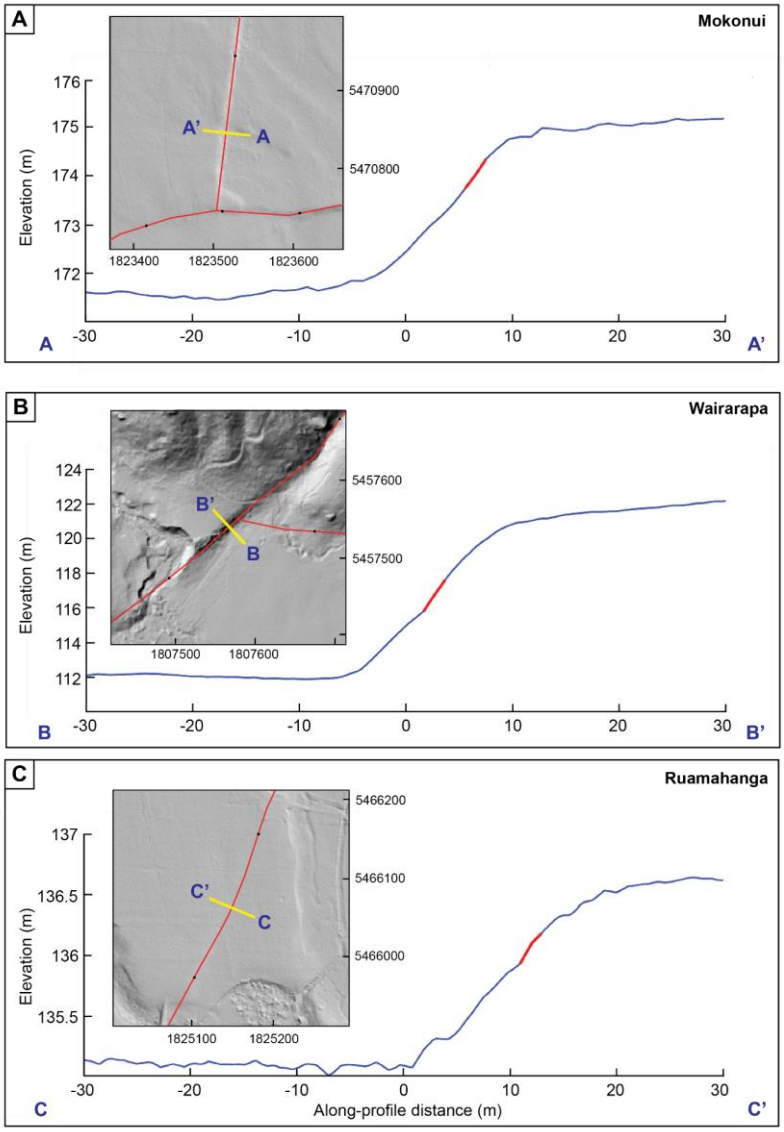

436 a

437 *Figure 7 – Examples of the method used to measure maximum fault scarp gradients. A) Mokonui Fault, B) Wairarapa*
438 *Fault, and C) Ruamahanga Fault. Insets show the fault sampled (red line), the yellow line is the orthogonal profile*
439 *along which scarp gradient was measured. The dark blue line is the profile extracted from the lidar data, and the part*
440 *of this line shown in red indicates the 2 m horizontal interval portion with the highest (steepest) gradient. Note the y-*
441 *axes for each profile are scaled differently.*

442 **Results**

443 ***Initial paleoseismic characterisation***

444 Our initial slip rate, SED and recurrence interval estimates for the Ruamahanga,

445 Carters Line, Pāpāwai, and Woodside faults are summarised in Figure 8 and Table 2 and

446 are described here.

Vertical offsets measured along three strands of the **Ruamahanga Fault** that cross Q2al, Q3al, and Q4al surfaces range from 0.7 to 5.1 m (Supplementary Table S1, Supplementary Table S2). These result in a vertical slip rate of 0.24 ± 0.2 mm/yr across the fault (Figure 8A). No horizontally offset features could be identified, however we cannot rule out a small component of horizontal offset, therefore this vertical slip rate should be considered a minimum bound on net slip rate. Using the overall length of the Ruamahanga Fault (7 km) and the scaling relationships from the previous section yields an average SED of 0.9 ± 0.5 m and a magnitude M_w of 6.3 for an earthquake that ruptures the entire fault. From this, the SED and the measured minimum net slip rate for the Ruamahanga Fault leads to a maximum recurrence interval of 6700 years (Table 2). This magnitude derived for the Ruamahanga Fault is below what is required for observable evidence of surface rupture in A-NZ (Coffey et al., 2022; Nicol, Van Dissen, et al., 2016), indicating that this fault likely does not rupture on its own and instead co-ruptures with other nearby faults.

Vertical slip rates were calculated for two locations along the **Woodside Fault**, both on the Waiohine terrace, Q2al (Figure 8C). These two transects crossed three strands of the Woodside Fault, yielding vertical offsets that range from 30 cm to 1.9 m (Supplementary Table 1, Supplementary Table S2) leading to vertical slip rates of 0.2 ± 0.07 mm/yr and 0.1 ± 0.06 mm/yr (Figure 8C). Additionally, two horizontal offsets of 9 ± 2.5 m and 5.5 ± 2 m were identified along a Q2al terrace riser, across different strands of the Woodside Fault (Figure 8C; Supplementary Figure S3). These result in horizontal slip rates of 0.8 ± 0.3 mm/yr and 0.3 ± 0.2 mm/yr, respectively. Summing these horizontal slip rates across the two strands results in a total horizontal slip rate of 1.1 ± 0.43 mm/yr, which leads to an average net slip rate of 1.1 ± 0.4 mm/yr, the highest slip rate among the four newly identified faults discussed here. Using its length of 6 km, scaling relationships

result in an average SED of 0.8 ± 0.5 m and a magnitude M_w of 6.2 for the Woodside Fault. SED and net slip rate were used to calculate a recurrence interval of 770 ± 540 years (Table 2), the shortest of those calculated along the four faults covered here. Similar to the Ruamahanga Fault, the magnitude calculated for the Woodside fault is below the threshold for surface rupture detection (Coffey et al., 2022; Nicol, Van Dissen, et al., 2016). This coupled with its short recurrence interval suggests that it too is predominantly with involved in multi-fault ruptures and likely co-ruptures with the Wairarapa Fault.

Vertical slip rates were measured at two locations along the **Carters Line Fault**, where Q2al and Q5al surfaces are offset by 30 cm - 17 m (Supplementary Table S1, Supplementary Table S2). A vertical slip rate of 0.1 ± 0.03 mm/yr is calculated towards the southwest while a higher slip rate of 0.24 ± 0.2 mm/yr was calculated further northeast (Figure 8D). No horizontal offsets were identified along the Carters Line Fault, and we are likely missing a considerable component of its net slip particularly along east-west striking traces. Consequently, we interpret the smaller vertical slip rate to be a minimum net slip rate and with a length of 18 km, the Carters Line Fault has an average SED of 1.4 ± 0.8 m, a magnitude of M_w of 6.7, and a maximum recurrence interval of 14,000 years (Table 2). Like the Woodside and Ruamahanga faults, this magnitude suggests the Carters Line Fault too predominantly participates in multi-fault earthquakes.

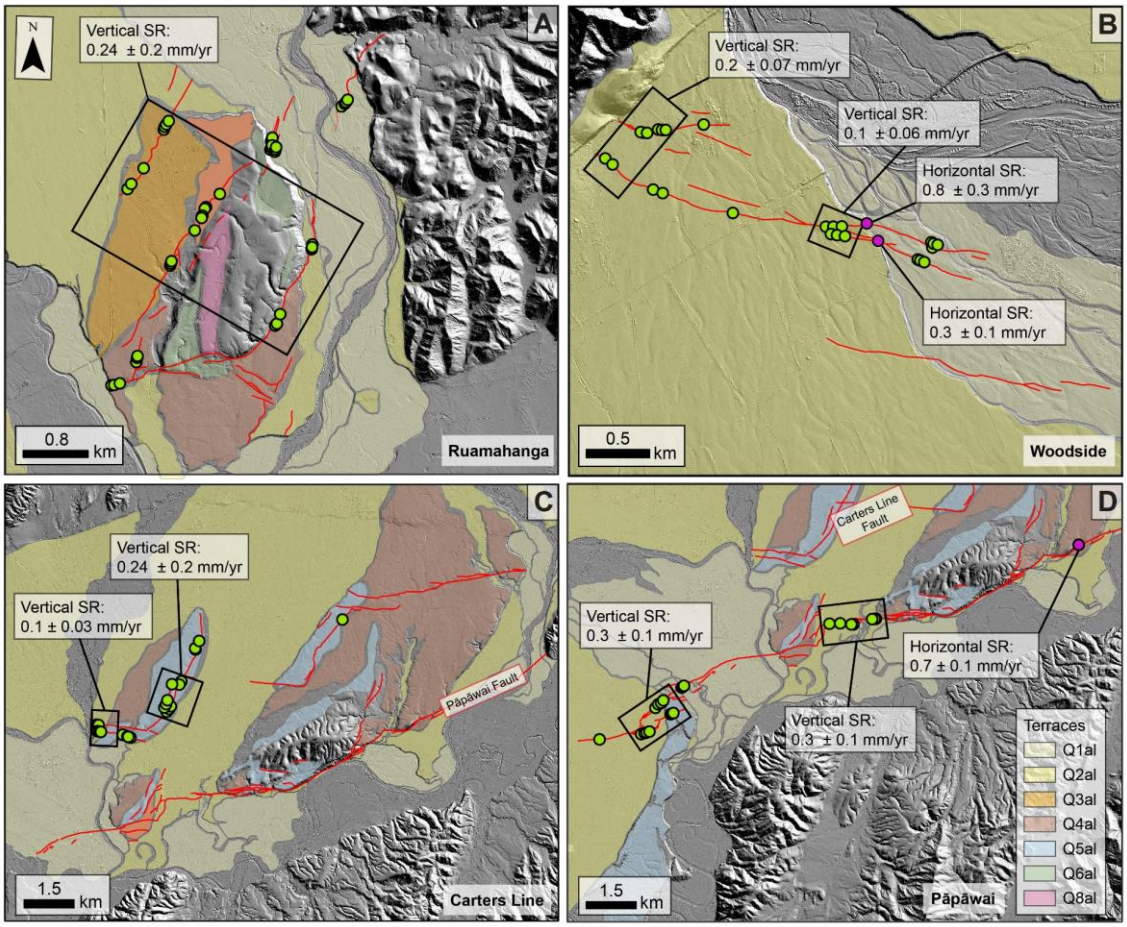

Figure 8- Summary of slip rates calculated for the A) Ruamahanga, B) Woodside, C) Carters Line, and D) Pāpāwai faults Green points indicate locations where a vertical slip rate was measured, and magenta points indicate where a horizontal slip rate was measured. Black rectangles delineate where an average slip rate was calculated from individual slip rate measurements and summed across multiple strands.

Vertical slip rates were calculated at two locations along the **Pāpāwai Fault** (Figure 8B) on a Q2al surface. Here the Pāpāwai Fault offsets this surface by 0.5 – 5 m (Supplementary Table S1, Supplementary Table S2) and the resulting vertical slip rates for both locations are 0.3 ± 0.1 mm/yr. A horizontal offset of 38 m ± 6 m along the Pāpāwai Fault was identified towards its eastern end (Figure 8B) on a Q4al terrace riser. Back slipping this offset and applying the age of abandonment of the Q4al terrace leads to a horizontal slip rate of 0.7 ± 0.1 mm/yr (Figure 8B; Supplementary Figure S4). These vertical and horizontal slip rates result in a net slip rate of 0.8 ± 0.1 mm/yr for the Pāpāwai Fault, which, along with a length of 26 km result in an average SED of 1.7 ± 1 m, a

magnitude of M_w 6.9 and a recurrence interval of 2200 ± 1200 years (Table 2). The resulting magnitude is on the edge of what is expected to generate detectable surface rupture (Coffey et al., 2022; Nicol, Van Dissen, et al., 2016), suggesting that the Pāpāwai Fault too, may have ruptured as part of previous multi-fault earthquakes in the Wairarapa Region.

In summary, our initial constraints on net slip rate and recurrence interval for the Ruamahanga, Pāpāwai, Woodside, and Carters Line faults range from 0.1 to 1.1 mm/yr and 770 to < 15,000 years respectively (Table 2). These broadly span the slip rates and recurrence intervals of the Masterton, Mokonui, and Carterton faults, which are 0.2 – 3 mm/yr and 2000 – 3500 years, respectively (Begg et al., 2001; Langridge et al., 2003; Litchfield et al., 2023; Seebeck et al., 2023; Townsend et al., 2002; Zachariesen et al., 2000). Estimates of magnitudes calculated for each of these four faults fall between M_w 6.3 to 6.9, which is lower than the minimum magnitude we expect to detect surface rupture for faults in A-NZ (M_w 7) (Coffey et al., 2022; Nicol, Van Dissen, et al., 2016). This suggests we may be underestimating the magnitude and average SED along these four faults and that they have ruptured as part of multi-fault events in the past. However, we emphasise that the constraints developed here are from desktop investigation and that further paleoseismic interrogation should be undertaken to refine these.

Table 2 – Slip rates (SR), single event displacements (SEDs), recurrence intervals (RI) and moment magnitudes (M_w) calculated for the four newly mapped faults.

Fault	Vertical SR (mm/yr)	Horizontal SR (mm/yr)	Net SR (mm/yr)	SED (m)	RI (years)	M_w	Length (km)
Ruamahanga	0.2 ± 0.2	-	>0.2 ± 0.2	0.9 ± 0.5	< 6700	6.3	7
Woodside	0.2 ± 0.07	1.1 ± 0.4	1.1 ± 0.4	0.8 ± 0.5	770 ± 540	6.2	6
Carters Line	0.1 ± 0.03 0.2 ± 0.2	-	> 0.1	1.4 ± 0.8	< 14000	6.7	18
Pāpāwai	0.3 ± 0.1	0.7 ± 0.1	0.8 ± 0.1	1.7 ± 1	2200 ± 1200	6.9	26

Fault scarp gradients and implications for past multi-fault ruptures

The lidar-based fault mapping showed that several of the faults in the Wairarapa Valley have very sharp scarps and this was confirmed by the fault scarp gradient analysis shown in Figure 9. Unsurprisingly, the fault with the steepest normalised scarp gradients is the Wairarapa Fault, since it ruptured in 1855 CE, and therefore it can be used for relative calibration against other faults. Steeper gradients tend to occur along simpler sections of the Wairarapa Fault where rupture (and strain) is localised onto fewer strands. This analysis also shows that the Mokonui Fault has steeper scarp gradients along its length compared to other faults across the valley. The steepest of these gradients occur along the eastern north-south striking 'train-track' scarps (Figure 6D-E), while the gentlest relief occurs north of here where the Mokonui Fault transitions to lower angle thrust faulting (Figure 6F-G). The Ruamahanga, Masterton, Carterton, Carters Line, Pāpāwai, and Woodside faults all have lower normalised scarp gradients except for the southwestern part of the Carterton Fault (orange points in Figure 9), which instead demonstrates steeper scarp gradients although not as steep as those measured on the Mokonui Fault.

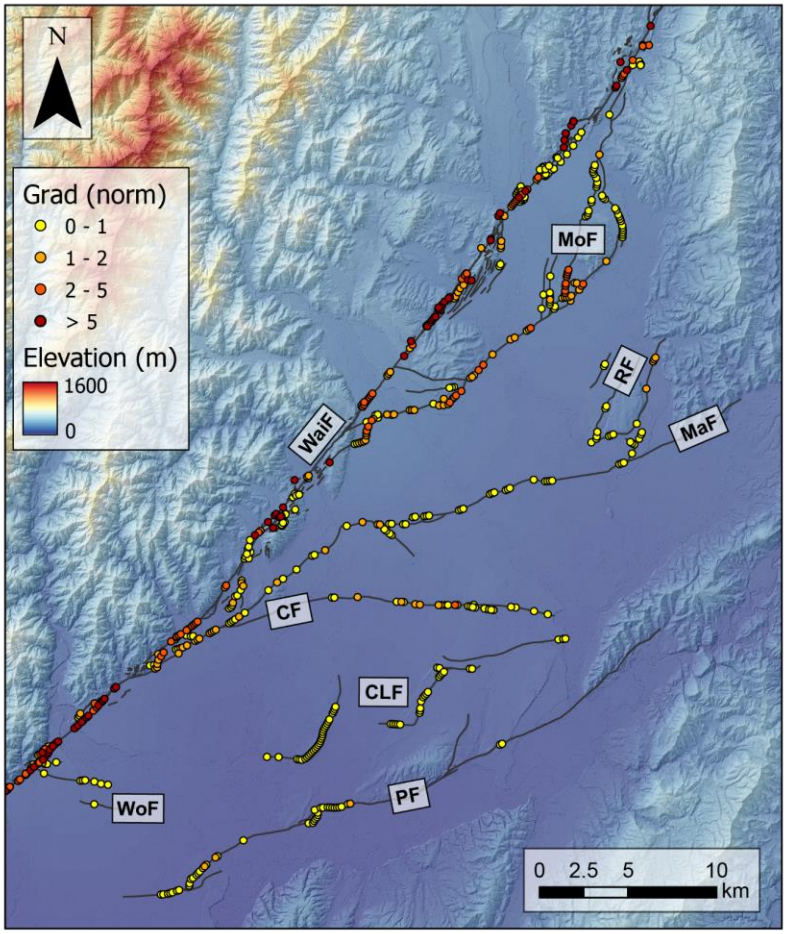

Figure 9 – Normalised fault scarp gradient data for faults in the northern Wairarapa Valley. Warmer colours indicate steeper gradients. Faults are shown as grey lines and are as follows: Wairarapa Fault (WaiF), Mokonui Fault (MoF), Ruamahanga Fault (RF), Masterton Fault (MaF), Carterton Fault (CF), Carters Line Fault (CLF), Pāpāwai Fault (PF), Woodside Fault (WoF).

Discussion

Implications of new mapping on interpretation of fault kinematics

New high-resolution mapping of active faults in the Wairarapa Region has shown that the expression of surface faulting is more complex than previously appreciated, both due to a greater number of active fault traces (including previously unidentified faults), as well as a greater range of fault geometries. For the newly mapped traces, 40 km has been added to the Wellington Fault, due mainly to the increased sinuosity of the main trace and to the additional subsidiary traces. This increased complexity is possibly due to the Wellington Fault traversing Torlesse Terrane basement, with traces forming due to slip on pre-existing basement structures, and/or because a longer period of faulting may

559 be preserved compared to younger surfaces. Furthermore, lidar allows for a more detailed
560 view of surface faulting beneath forest cover, permitting a more complex array of faulting
561 to be observed.

562 Some other faults show greater complexity in areas of geometric change, either
563 where there is splay faulting or where there is a change in fault strike. For example where
564 the Masterton, Carterton, and Mokonui faults branch off the Wairarapa Fault, or where
565 the Pāpāwai Fault transitions from being northeast striking to more north striking (Figure
566 5E). The same correlation has been observed in previous studies where distributed active
567 faulting has been proposed to act as a linkage between different fault segments (Ben-Zion
568 & Sammis, 2003; Iezzi et al., 2023; Petersen et al., 2011). It has also been noted from
569 past historic earthquakes, such as the 2010 M_W 7.1 Darfield earthquake, that
570 unconsolidated sediments like those present in the Wairarapa Valley, may favour more
571 distributed surface rupture compared to bedrock faults (Milliner et al., 2015; Quigley et
572 al., 2011; Quigley et al., 2010; Teran et al., 2015); and this may also play a role in
573 facilitating distributed deformation observed along faults across the Wairarapa Valley.

574 On a regional scale the newly identified faults are generally located in gaps
575 between the previously mapped major faults in the Wairarapa Valley (Wellington,
576 Wairarapa, Mokonui, Masterton, Carterton) with additional faults branching from the
577 Wairarapa Fault (in a horsetail fashion). At the scale of individual faults the Carters Line,
578 Pāpāwai and Ruamahanga faults show partitioning into reverse northeast-southwest
579 striking traces and dextral strike-slip west-east striking traces, suggesting that they could
580 be immature faults forming between the larger faults and some may be reactivated
581 bedrock structures (e.g. in Torlesse terrane basement). Similar slip partitioning occurred
582 in the epicentral region of the 2016 Kaikōura earthquake. North to north-northeast-
583 striking faults that exploit bedding planes in the Torlesse terrane hosted more reverse

584 displacement, while predominantly right-lateral reverse displacement was accommodated
585 on northeast-striking faults (Nicol et al., 2018). This slip partitioning during the Kaikōura
586 earthquake has been attributed to a model of transpression put forward by Dewey et al.
587 (1998) influenced by pre-existing basement heterogeneity (Nicol et al., 2018), which may
588 also explain observations of slip portioning across the Wairarapa Valley.
589 Revisions to the western end of the Masterton and Carterton Faults shows that the
590 Masterton Fault does not directly connect to the Wairarapa Fault, but instead connects to
591 the Carterton Fault. Previously, the Carterton Fault was mapped as a single structure
592 extending from the Wairarapa Valley into the Coastal Range (referred to here as the
593 Eastern Carterton Fault) (Figure 3B), but the Carters Line and Pāpāwai faults also
594 converge towards the Carterton Fault in the Coastal Range. From a purely geometric
595 perspective, the Pāpāwai Fault is more aligned with the eastern part of the Carterton Fault,
596 suggesting that they collectively could be expressions of the same throughgoing structure.
597 If this is the case, then the total length of the Pāpāwai Fault increases from 26 km to 53
598 km and, using the methodologies described earlier, the SED, magnitude and recurrence
599 interval for the Pāpāwai Fault increases to 2.5 ± 1.4 m, M_w 7.2, 3100 ± 1800 years
600 respectively (Supplementary table S3).
601 In the tectonic block models of Wallace et al. (2004) and Wallace et al. (2012), 5
602 mm/yr of strain is accommodated across valley-cutting splay faults (Mokonui, Carterton,
603 and Masterton faults), which facilitates a transition to lower slip rate along the Northern
604 Wairarapa Fault. This can be interrogated using updated fault mapping and paleoseismic
605 constraints. Based upon this, we suggest that the Mokonui Fault should be treated as part
606 of the Wairarapa Fault when considering these block boundaries and that the Pāpāwai
607 and Carters Line faults should be considered alongside the Masterton and Carterton faults.
608 Consequently, summing the mean geological slip rates of the Masterton and Carterton

faults from the CFM (Seebeck et al., 2023) and the mean slip rates calculated here for the newly mapped Pāpāwai and Carters Line Fault results in a distributed boundary slip rate of > 4.8 mm/yr (Supplementary Figure S6), consistent with that derived in Wallace et al. (2012).

How many faults ruptured in the 1855 AD Wairarapa Earthquake?

Fault scarp gradient measurements showed that the Wairarapa Fault has the steepest fault scarps in the northern Wairarapa Valley, followed by the Mokonui Fault, and the western end of the Carterton Fault (Figure 9). We suggest that high values of normalised scarp gradient suggest that the fault has likely experienced recent surface rupture (Hodge et al., 2019; Middleton et al., 2016). While this analysis does not definitively tell us whether a fault has ruptured recently (i.e. historically), it does provide us with a means of quantifying more qualitative observations of steep scarp relief that were made during fault mapping, which can be used to make inferences about the extent of past multi-fault rupture. We explore the possibility of past upper plate multi-fault rupture here, but it is important to note that we have not considered joint rupture of upper-plate faults with the Hikurangi subduction interface (e.g. Humphrey et al. 2025).

The high normalised scarp gradients measured along the Wairarapa Fault were expected and are taken here as reflecting rupture in the 1855 CE Wairarapa Earthquake (Rodgers & Little, 2006). Similarly steep scarp gradients on the Mokonui Fault suggest that it could have ruptured during the 1855 CE Wairarapa Earthquake. This is consistent with its geomorphic relationship with the Wairarapa Fault, where it branches off the Wairarapa Fault at its southern extent before rejoining it further north, suggesting the two faults are geometrically and kinematically linked. Recent rupture of the Mokonui fault is also supported by its surface morphology at its northern end where it transitions to lower angle

633 thrust faulting (Figure 6F, G). Here, the Mokonui Fault has a scalloped morphology with
634 small-scale changes in its trend reflecting changes in its fault plane geometry and the
635 presence of abandoned channels of the young Q1al surface. We expect that the gently
636 sloping scarp with its short wavelength changes in fault strike, would be eroded relatively
637 quickly from the landscape, therefore the preservation of these features likely means that
638 not much time has elapsed since its most recent surface rupture. It is unlikely that the
639 Mokonui Fault ruptured with some lag after the 1855 CE Wairarapa Earthquake as there
640 are no reports of another large earthquake in the Wairarapa Valley at this time. It is,
641 however, possible that the last rupture of the Mokonui Fault preceded the 1855 CE
642 Wairarapa Earthquake, prior to the European settlement of A-NZ in the 1840s. However,
643 mapping shows that the Mokonui Fault is kinematically linked to the Wairarapa Fault,
644 therefore we expect that some coseismic slip along the Wairarapa Fault would be
645 partitioned along the Mokonui Fault. Furthermore, previous work has also posed that
646 other faults in the southern North Island and Cook Strait ruptured during the 1855 CE
647 Wairarapa Earthquake (Holdgate & Grapes, 2014; Little et al., 2009; Schermer et al.,
648 2004). In addition to co-rupture of the Mokonui and Wairarapa faults, we also suggest
649 that steep scarp gradients along the southwestern part of the Carterton Fault (where it is
650 closest to the Wairarapa Fault) mean that it too may have partially ruptured during the
651 1855 CE earthquake, with rupture extending at least 5 km along the Carterton Fault from
652 its junction with the Wairarapa Fault (Supplementary Figure S8). Our results along with
653 previous work suggest a tendency for ruptures in the Wairarapa Valley to be more
654 complex involving multiple faults, perhaps analogous to the 2016 Kaikōura earthquake
655 where strain partitioning also plays a key role in fault kinematics of the area (Nicol et al.,
656 2018).

In addition to fault scarp gradients, paleoseismic constraints also provide some insight into potential multi-fault rupture. The Woodside Fault has an anomalously short recurrence interval compared to other faults across the valley, which have recurrence intervals that are more than twice as long (Table 2). This is a consequence of how recurrence interval was calculated here, where weight is placed on the short length of the Woodside Fault and its relatively large horizontal offsets, which together suggests that the Woodside Fault does not rupture on its own. Instead, it may rupture with either/both the Wairarapa or Carters Line faults. On top of this, magnitude length scaling relationships suggest the Carters Line, Ruamahanga, Woodside, and Pāpāwai faults have magnitudes corresponding to whole-fault rupture that range between M_w 6.1 to M_w 6.9. These magnitudes are below what is generally considered to produce detectable surface rupture in New Zealand and suggests that all four of these faults have been involved in multi-fault ruptures in the past (Coffey et al., 2022; Nicol, Robinson, et al., 2016).

Implications for fault models

Results of the updated mapping completed in the Wairarapa region should be incorporated in future iterations of the CFM (Seebeck et al., 2023) and we outline some of these potential changes here. We recommend the addition of twelve faults, the: Battery Hill, Flat Point, Mangaoranga, Mangaterere, Pāpāwai, Pirinoa, Ruamahanga, Wharekauhau East, Woodside, Motumatai, Te Hau, and Carters Line faults; along with modifications to nine others (Mokonui, Carterton, Masterton, Te Maire, Flat Point, Kaumingi, Martinborough, Dry River, and Huangarua faults), and removal of the Ngāpotiki Fault. Sections along the Wellington and Wairarapa faults remain unchanged. These suggested changes to the Wairarapa CFM are presented in Figure 10 and in the Supplementary Materials, but key changes are summarised below on a fault-by-fault basis

681 below. Updated attributes are presented in Supplementary Table S3.

682 The northeastern section of the Mokonui Fault, where it extends through the
683 Coastal Range, has been removed and, instead, it is continued to the north to connect back
684 to the Wairarapa Fault. Updated lidar-based mapping confirms the presence of active fault
685 traces in the Coastal Range (Figure 3B); however, these are relatively short and do not
686 appear to be the extensions of the Mokonui Fault, therefore they are left unnamed and not
687 included in Figure 10. An alternative interpretation would be to add an additional
688 northeast-southwest trending fault here to reflect these traces in the Coastal Range. In
689 addition to inclusion of the Woodside and Carters Line faults, we suggest that these two
690 faults are connected to form a single structure, referred to as the Woodside-Carters Line
691 Fault, due to their proximity and similarity in orientation. In this scenario the magnitude
692 of single-fault ruptures on the Woodside-Carters Line Fault is calculated to be M_w 6.8,
693 slightly higher than those earthquakes that are solely on the Carters Line Fault (M_w = 6.7),
694 while the SED increases to 1.6 ± 0.9 m and RI to a poorly constrained 1500 ± 1080 years
695 (Supplementary Table S3). An alternative option is that the Woodside Fault is not
696 included, but instead due to its length, is inferred to be part of the Wairarapa Fault at the
697 scale of the CFM, while the Carters Line Fault is included where it is mapped. The
698 Pāpāwai Fault has been connected to the eastern Carterton Fault and we refer to this entire
699 structure as the Pāpāwai Fault. Consequently, the Carterton Fault is shortened by ~50 km
700 and no longer extends through the Coastal Range. This is our preferred interpretation
701 based upon similarities in their geometry but note that there is uncertainty in this.
702 Alternative possible scenarios include that the eastern Carterton Fault is connected to the
703 Carterton Fault, as was previously inferred, or that it is connected to the Carters Line
704 Fault. Additionally, to reflect updated mapping, the southwestern end of the Masterton
705 Fault has been adjusted so that it now branches off the Carterton Fault. Its traces to the

east have also been shifted southwards close to its intersection with the Ruamahanga Fault. The Te Maire Fault has been shifted 2-3 km to the west to better reflect the location of most mapped traces on the west side of Bidwill Hill. Southeast of there, the Martinborough Fault has been shifted slightly west so that it more closely aligns with observed surface traces and the newly mapped Morison Hill Fault. The previously inferred Dry River-Huangarua Fault has been separated into two faults, as the sharpness of the Huangarua Fault suggests that it is considerably more active than the Dry River Fault. The Flat Point and Kaumingi faults have been shortened to reflect the extent of their mapped surface traces, but they may have greater length at depth. Finally, the Ngāpotiki Fault has been removed due to the absence of any evidence of surface rupture.

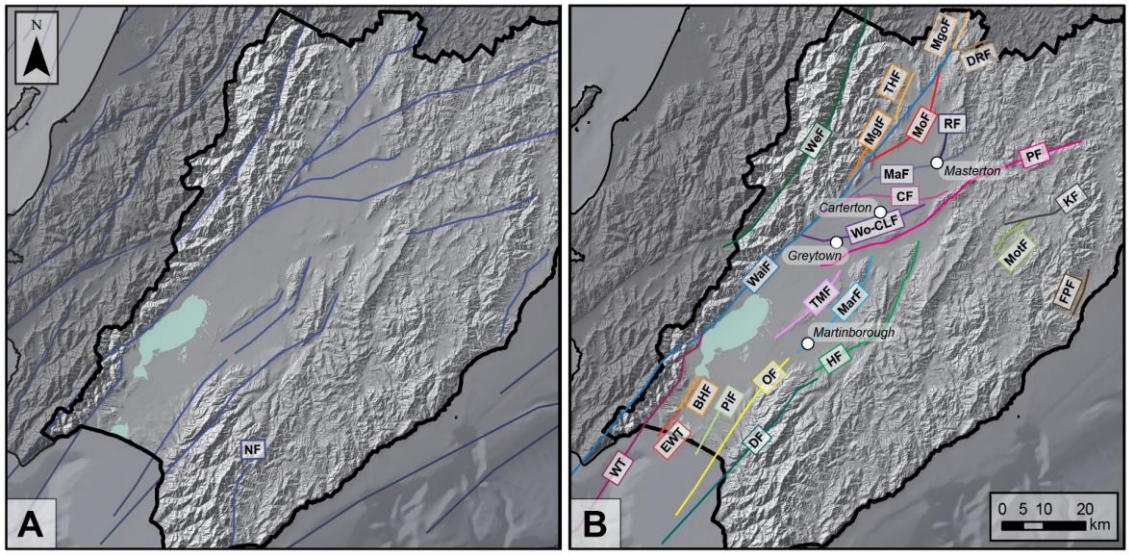

Figure 10 – A) Version 1.0 of the NZ CFM (Seebeck et al. 2024). B) Suggested revision of the CFM in the Wairarapa following the results of the active fault mapping presented here. The faults are as follows: MgoF – Mangaoranga Fault, DRF – Dry River Fault, THF – Te Hau Fault, MoF – Mokonui Fault, MgtF – Mangatoro Fault, MaF – Masterton Fault, RF – Ruamahanga Fault, CF – Carterton Fault, WeF – Wellington Fault, PF – Pāpāwai Fault, Wo-CLF – Woodside-Carters Line Fault, KF – Kaumingi Fault, MotF – Motumatai Fault, WaiF – Wairarapa Fault, FPF – Flatpoint Fault, TMF – Te Maire Fault, MarF – Martinborough Fault, HF – Huangarua Fault, OF – Otaraia Fault, DF – Dry River Fault, PiF – Pirinoa Fault, BHF – Battery Hill Fault NF - Ngāpotiki, EWT – Eastern Wharekauhau Thrust, and WT – Wharekauhau Thrust. A shapefile with the suggested update to the NZ CFM is included in the Supplementary Materials.

Summary and Conclusions

New mapping of active faults in the Wairarapa Region using lidar data has led to

the identification of many new fault traces along previously known active faults and the discovery of seven previously unrecognised faults. Four of these faults are described here and have preliminary slip rates and recurrence intervals that fall between 0.1-1.1 mm/yr and 770-14,000 years respectively. Fault mapping has revealed more distributed deformation across faults in the Wairarapa, particularly within areas associated with changes in fault geometry. Sharp fault scarps have been identified and normalised slope gradients suggest that the 1855 CE Wairarapa Earthquake may have included rupture of the Mokonui Fault and the western end of the Carterton Fault, further supporting the occurrence of multi-fault rupture in A-NZ. Updates to fault mapping have been translated to proposed changes to the A-NZ CFM in the Wairarapa Region and may impact its seismic hazard if incorporated in future revisions of the NSHM. However, many faults in the Wairarapa do not have well-characterised paleoseismic constraints. Consequently, further work is needed to refine these constraints, particularly for faults close to population centres, is required to better define and understand the seismic hazard posed to nearby communities.

Acknowledgements

We are grateful to the Its Our Fault programme for funding a lot of the work that makes up this manuscript, along with funding from the Hazards and Risk Management Programme (Strategic Science Investment Fund contract C05X1702). We also acknowledge and thank Russ Van Dissen for reading this manuscript and providing valuable feedback, as well as Jesse Kearse and Andy Nicol for providing useful comments and changes during the peer review process.

Data availability statement

Updated active fault mapping discussed in this manuscript is viewable on the GNS Science high resolution dataset of the New Zealand Active Faults Database (Morgenstern et al., 2024), Wairarapa Maps Online, and Greater Wellington Maps Viewer (Hazards and Emergency Management). A shapefile of the updated mapping can be provided upon request. All additional data can be found in the supplementary materials

References

Bailleul, J., Robin, C., Chanier, F., Guillocheau, F., Field, B., & Ferriere, J. (2007). Turbidite Systems in the Inner Forearc Domain of the Hikurangi Convergent Margin (New Zealand): New Constraints on the Development of Trench-Slope Basins. *Journal of Sedimentary Research*, *77*(4), 263-283. https://doi.org/10.2110/jsr.2007.028

Barnes, P. M., Lamarche, G., Bialas, J., Henrys, S., Pecher, I., Netzeband, G. L., Greinert, J., Mountjoy, J. J., Pedley, K., & Crutchley, G. (2010). Tectonic and geological framework for gas hydrates and cold seeps on the Hikurangi subduction margin, New Zealand. *Marine Geology*, *272*(1-4), 26-48. https://doi.org/10.1016/j.margeo.2009.03.012

Beanland, S., Berryman, K. R., & Blick, G. H. (1989). Geological investigations of the 1987 Edgecumbe earthquake, New Zealand. *New Zealand Journal of Geology and Geophysics*, *32*(1), 73-91. https://doi.org/10.1080/00288306.1989.10421390

Beanland, S., Melhuish, A., Nicol, A., & Ravens, J. (1998). Structure and deformational history of the inner forearc region, Hikurangi subduction margin, New Zealand. *New Zealand Journal of Geology and Geophysics*, *41*(4), 325-342. https://doi.org/10.1080/00288306.1998.9514814

Beavan, J., Tregoning, P., Bevis, M., Kato, T., & Meertens, C. (2002). Motion and rigidity of the Pacific Plate and implications for plate boundary deformation. *Journal of Geophysical Research: Solid Earth*, *107*(B10). https://doi.org/10.1029/2001jb000282

Begg, J., Villamor, P., Zachariesen, J., & Litchfield, N. (2001). *Paleoseismic assessment of the active Masterton and Carterton faults, Wairarapa* (GNS Science client report, Issue 2001/70).

Begg, J. G., & Johnston, M. R. (2000). *Geology of the Wellington area* [1:250 000 geological map 10]. Lower Hutt, New Zealand, Institute of Geological and Nuclear Sciences.

Ben-Zion, Y., & Sammis, C. G. (2003). Characterization of fault zones. *Pure and Applied Geophysics*, *160*, 677-715.

Berryman, K. R. (1980). Late Quaternary movement on White Creek Fault, South Island, New Zealand. *New Zealand Journal of Geology and Geophysics*, *23*(1), 93-101. https://doi.org/10.1080/00288306.1980.10424194

Cape, C. D., Lamb, S. H., Vella, P., Wells, P. E., & Woodward, D. J. (1990). Geological structure of Wairarapa Valley, New Zealand, from seismic reflection profiling. *Journal of the Royal Society of New Zealand*, *20*(1), 85-105. https://doi.org/10.1080/03036758.1990.10426734

Carne, R. C., Little, T. A., & Rieser, U. (2011). Using displaced river terraces to determine Late Quaternary slip rate for the central Wairarapa Fault at Waiohine River, New Zealand. *New Zealand Journal of Geology and Geophysics*, *54*(2), 217-236. https://doi.org/10.1080/00288306.2010.532224

Coffey, G. L., & Litchfield, N. J. (2023). *Ground truthing and preliminary slip rates and recurrence intervals for four newly identified faults in the Wairarapa Region* (GNS Science report, Issue 2023/39).

Coffey, G. L., Rollins, C., Van Dissen, R. J., Rhoades, D. A., Gerstenberger, M. C., Litchfield, N. J., & Thingbaijam, K. K. S. (2023). Paleoseismic Earthquake Recurrence Interval Derivation for the 2022 Revision of the New Zealand National Seismic Hazard Model. *Seismological Research Letters*, *95*(1), 78-94. https://doi.org/10.1785/0220230197

Coffey, G. L., Rollins, C., Van Dissen, R. J., Rhoades, D. A., Thingbaijam, K. K. S., Clark, K. J., Gerstenberger, M. C., Litchfield, N. J., & Nicol, A. (2022). *New Zealand National Seismic Hazard Model 2022: Earthquake recurrence derivation from paleoseismic data and probability of detection* (GNS Science Report, Issue.

Darby, D., & Beavan, J. (2001). Evidence from GPS measurements for contemporary interplate coupling on the southern Hikurangi subduction thrust and for partitioning of strain in the upper plate. *Journal of Geophysical Research: Solid Earth*, *106*(B12), 30881-30891. https://doi.org/10.1029/2000jb000023

DeMets, C., Gordon, R. G., Argus, D. F., & Stein, S. (1990). Current plate motions. *Geophysical Journal International*, *101*(2), 425-475.

Dewey, J. F., Holdsworth, R. E., Strachan, R. A. . (1998). Transpression and transtension zones. *Continental Transpressional and Transtensional Tectonics*, *135*, 1-14.

Ellis, S., Bannister, S., Van Dissen, R., Eberhart-Phillips, D., Boulton, C., Reyners, M., Funnell, R., Mortimer, N., Upton, P., Rollins, C., & Seebeck, H. (2023). New Zealand Fault-Rupture Depth Model v.1.0: A Provisional Estimate of the Maximum Depth of Seismic Rupture on New Zealand's Active Faults. *Bulletin of the Seismological Society of America*, *114*(1), 78-94. https://doi.org/10.1785/0120230166

Formento-Trigilio, M. L., Burbank, D. W., Nicol, A., Schulmeister, J., & Rieser, U. (2002). River response to an active fold-and-thrust belt in a convergent margin setting, North Island, New Zealand. *Geomorphology*, *49*, 125-152.

Gerstenberger, M. C., Bora, S., Bradley, B. A., DiCaprio, C., Kaiser, A., Manea, E. F., Nicol, A., Rollins, C., Stirling, M. W., Thingbaijam, K. K. S., Van Dissen, R. J., Abbott, E. R., Atkinson, G. M., Chamberlain, C., Christophersen, A., Clark, K., Coffey, G. L., de la Torre, C. A., Ellis, S. M., . . . Wotherspoon, L. M. (2024). The 2022 Aotearoa New Zealand National Seismic Hazard Model: Process, Overview, and Results. *Bulletin of the Seismological Society of America*, *114*(1), 7-36. https://doi.org/10.1785/0120230182

Gerstenberger, M. C., Van Dissen, R., Rollins, C., DiCaprio, C., Thingbaijim, K. K. S., Bora, S., Chamberlain, C., Christophersen, A., Coffey, G. L., Ellis, S. M., Iturrieta, P., Johnson, K. M., Litchfield, N. J., Nicol, A., Milner, K. R., Rastin, S. J., Rhoades, D., Seebeck, H., Shaw, B. E., . . . Williams, C. (2024). The Seismicity Rate Model for the 2022 Aotearoa New Zealand National Seismic Hazard Model. *Bulletin of the Seismological Society of America*, *114*(1), 182-216. https://doi.org/10.1785/0120230165

Grapes, R. H., & Downes, G. (1997). The 1855 Wairarapa, New Zealand, earthquake - analysis of historical data. *Bulletin of the New Zealand Society for Earthquake Engineering*, *30*(4), 271-367.

Hamling, I. J., Hreinsdottir, S., Clark, K., Elliott, J., Liang, C., Fielding, E., Litchfield, N., Villamor, P., Wallace, L., Wright, T. J., D'Anastasio, E., Bannister, S., Burbidge, D., Denys, P., Gentle, P., Howarth, J., Mueller, C., Palmer, N., Pearson, C., . . . Stirling, M. (2017). Complex multifault rupture during the 2016 M(w) 7.8 Kaikoura earthquake, New Zealand. *Science*, *356*(6334). https://doi.org/10.1126/science.aam7194

Heron, D. W. (2023). *Geological Map of New Zealand 1:250,000*. Lower Hutt, GNS Science.

Hodge, M., Biggs, J., Fagereng, Å., Elliott, A., Mdala, H., & Mphepo, F. (2019). A semi-automated algorithm to quantify scarp morphology (SPARTA): application

to normal faults in southern Malawi. *Solid Earth*, *10*(1), 27-57. https://doi.org/10.5194/se-10-27-2019

Hodge, M., Biggs, J., Fagereng, Å., Mdala, H., Wedmore, L. N. J., & Williams, J. N. (2020). Evidence From High-Resolution Topography for Multiple Earthquakes on High Slip-to-Length Fault Scarps: The Bilila-Mtakataka Fault, Malawi. *Tectonics*, *39*(2). https://doi.org/10.1029/2019tc005933

Holdgate, G. R., & Grapes, R. H. (2014). Wairau Basin and fault connections across Cook Strait, New Zealand: seismic and geological evidence. *Australian Journal of Earth Sciences*, *62*(1), 95-121. https://doi.org/10.1080/08120099.2015.986195

Howell, A., Nissen, E., Stahl, T., Clark, K., Kearse, J., Van Dissen, R., Villamor, P., Langridge, R., & Jones, K. (2020). Three-Dimensional Surface Displacements During the 2016 MW 7.8 Kaikōura Earthquake (New Zealand) From Photogrammetry-Derived Point Clouds. *Journal of Geophysical Research: Solid Earth*, *125*(1). https://doi.org/10.1029/2019jb018739

Humphrey, J., Nicol, A., Howell, A., Litchfield, N., Langridge, R., Van Dissen, R., Penney, C., & Fry, B. (2025). Spatial and Temporal Clustering of Large Earthquakes on Upper-Plate and Subduction Thrust Faults Along the Southern Hikurangi Subduction Margin, Aotearoa-New Zealand. *Bulletin of the Seismological Society of America*. https://doi.org/10.1785/0120240246

Iezzi, F., Francescone, M., Pizzi, A., Blumetti, A., Boncio, P., Di Manna, P., Pace, B., Piacentini, T., Papasodaro, F., Morelli, F., Caciagli, M., Chiappini, M., D'Ajello Caracciolo, F., Materni, V., Nicolosi, I., Sapia, V., & Urbini, S. (2023). Slip localization on multiple fault splays accommodating distributed deformation across normal fault complexities. *Tectonophysics*, *868*. https://doi.org/10.1016/j.tecto.2023.230075

Lamb, S. H., & Vella, P. (1987). The last million years of deformation in part of the New Zealand plate-boundary zone. *Journal of Structural Geology*, *9*(7), 877-891.

Langridge, R. M., Ries, W. F., Litchfield, N. J., Villamor, P., Van Dissen, R. J., Barrell, D. J. A., Rattenbury, M. S., Heron, D. W., Haubrock, S., Townsend, D. B., Lee, J. M., Berryman, K. R., Nicol, A., Cox, S. C., & Stirling, M. W. (2016). The New Zealand Active Faults Database. *New Zealand Journal of Geology and Geophysics*, *59*(1), 86-96. https://doi.org/10.1080/00288306.2015.1112818

Langridge, R. M., Townsend, D. B., & Persaud, M. (2003). *Paleoseismic assessment of the active Mokonui Fault, Wairarapa* (GNS Science client report, Issue 2003/68).

Lee, J. M., & Begg, J. G. (2002). *Geology of the Wairarapa area* [1:250 000 geological map 11]. Lower Hutt, New Zealand, Institute of Geological & Nuclear Sciences.

Litchfield, N. J., & Berryman, K. R. (2005). Correlation of fluvial terraces within the Hikurangi Margin, New Zealand: implications for climate and baselevel controls. *Geomorphology*, *68*(3-4), 291-313. https://doi.org/https://doi.org/10.1016/j.geomorph.2004.12.001

Litchfield, N. J., Coffey, G. L., & Morgenstern, R. (2022). *Active fault mapping for the South Wairarapa, Carterton, and Masterton districts* (GNS Science Consultancy report, Issue.

Litchfield, N. J., Humphrey, J., Morgenstern, R., Langridge, R. M., Coffey, G. L., & Van Dissen, R. J. (2023). The New Zealand Paleoseismic Site Database, Version 1.0. *Seismological Research Letters*, *95*(1), 64-77. https://doi.org/10.1785/0220230150

Little, T. A., Van Dissen, R., Schermer, E., & Carne, R. (2009). Late Holocene surface ruptures on the southern Wairarapa fault, New Zealand: Link between earthquakes and the uplifting of beach ridges on a rocky coast. *Lithosphere*, *1*(1), 4-28. https://doi.org/10.1130/l7.1

Middleton, T. A., Walker, R. T., Parsons, B., Lei, Q., Zhou, Y., & Ren, Z. (2016). A major, intraplate, normal-faulting earthquake: The 1739 Yinchuan event in northern China. *Journal of Geophysical Research: Solid Earth*, *121*(1), 293-320. https://doi.org/10.1002/2015jb012355

Milliner, C. W. D., Dolan, J. F., Hollingsworth, J., Leprince, S., Ayoub, F., & Sammis, C. G. (2015). Quantifying near-field and off-fault deformation patterns of the 1992 Mw 7.3 Landers earthquake. *Geochemistry, Geophysics, Geosystems*, *16*(5), 1577-1598. https://doi.org/10.1002/2014gc005693

Morgenstern, R., Litchfield, N. J., Langridge, R. M., Heron, D. W., Townsend, D. B., Villamor, P., Barrell, D. J. A., Ries, W. F., Van Dissen, R. J., Clark, K. J., Coffey, G. L., Zoeller, A., Howell, A., & Easterbrook-Clarke, L. H. (2024). New Zealand Active Faults Database: the high-resolution dataset v2.0. *New Zealand Journal of Geology and Geophysics*, 1-16. https://doi.org/10.1080/00288306.2024.2427396

Neef, G. (1995). Cretaceous and Cenozoic geology east of the Tinui Fault Complex in northeastern Wairarapa, New Zealand. *New Zealand Journal of Geology and Geophysics*, *38*(3), 375-394. https://doi.org/10.1080/00288306.1995.9514664

Nicol, A., & Beavan, J. (2003). Shortening of an overriding plate and its implications for slip on a subduction thrust, central Hikurangi Margin, New Zealand. *Tectonics*, *22*(6). https://doi.org/10.1029/2003tc001521

Nicol, A., Khajavi, N., Pettinga, J. R., Fenton, C., Stahl, T., Bannister, S., Pedley, K., Hyland-Brook, N., Bushell, T., Hamling, I., Ristau, J., Noble, D., & McColl, S. T. (2018). Preliminary Geometry, Displacement, and Kinematics of Fault Ruptures in the Epicentral Region of the 2016 Mw 7.8 Kaikōura, New Zealand, Earthquake. *Bulletin of the Seismological Society of America*, *108*(3B), 1521-1539. https://doi.org/10.1785/0120170329

Nicol, A., Narghes, K., Humphrey, J., Van Dissen, R., Gerstenberger, M., & Stirling, M. (2022). *Geometries and slip of historical surface-rupturing earthquakes in New Zealand and their application to seismic hazard analysis* (Final Report Biennial EQC Grant 16/718, Issue.

Nicol, A., Robinson, R., Van Dissen, R. J., & Harvison, A. (2016). Variability of recurrence interval and single-event slip for surface-rupturing earthquakes in New Zealand. *New Zealand Journal of Geology and Geophysics*, *59*(1), 97-116. https://doi.org/10.1080/00288306.2015.1127822

Nicol, A., Van Dissen, R. J., Stirling, M. W., & Gerstenberger, M. C. (2016). Completeness of the Paleoseismic Active-Fault Record in New Zealand. *Seismological Research Letters*, *87*(6), 1299-1310. https://doi.org/10.1785/0220160088

Nicol, A., VanDissen, R., Vella, P., Alloway, B., & Melhuish, A. (2002). Growth of contractional structures during the last 10 m.y. at the southern end of the emergent Hikurangi forearc basin, New Zealand. *New Zealand Journal of Geology and Geophysics*, *45*(3), 365-385. https://doi.org/10.1080/00288306.2002.9514979

Nicol, A., & Wallace, L. M. (2007). Temporal stability of deformation rates: Comparison of geological and geodetic observations, Hikurangi subduction

margin, New Zealand. *Earth and Planetary Science Letters*, *258*(3-4), 397-413. https://doi.org/10.1016/j.epsl.2007.03.039

Ninis, D., Little, T., Litchfield, N., Wang, N., Jacobs, K., & Henderson, C. M. (2022). Pleistocene marine terraces of the Wellington south coast – their distribution across multiple active faults at the southern Hikurangi subduction margin, Aotearoa New Zealand. *New Zealand Journal of Geology and Geophysics*, *65*(1), 242-263. https://doi.org/10.1080/00288306.2021.2011329

Nodder, S. D., Lamarche, G., Proust, J. N., & Stirling, M. (2007). Characterizing earthquake recurrence parameters for offshore faults in the low-strain, compressional Kapiti-Manawatu Fault System, New Zealand. *Journal of Geophysical Research: Solid Earth*, *112*(B12). https://doi.org/10.1029/2007jb005019

Palmer, A. S., Vucetich, C. G., McGlone, M., & Harper, M. A. (1989). Last Glacial loess and early Last Glacial vegetation history of Wairarapa Valley, New Zealand. *New Zealand Journal of Geology and Geophysics*, *32*, 499-513. https://doi.org/https://doi.org/10.1080/00288306.1989.10427557

Papanikolaou, I. D., Roberts, G. P., & Michetti, A. M. (2005). Fault scarps and deformation rates in Lazio–Abruzzo, Central Italy: Comparison between geological fault slip-rate and GPS data. *Tectonophysics*, *408*(1-4), 147-176. https://doi.org/10.1016/j.tecto.2005.05.043

Petersen, M. D., Dawson, T. E., Chen, R., Cao, T., Wills, C. J., Schwartz, D. P., & Frankel, A. D. (2011). Fault Displacement Hazard for Strike-Slip Faults. *Bulletin of the Seismological Society of America*, *101*(2), 805-825. https://doi.org/10.1785/0120100035

Quigley, M., Van Dissen, R., Litchfield, N., Villamor, P., Duffy, B., Barrell, D., Furlong, K., Stahl, T., Bilderback, E., & Noble, D. (2011). Surface rupture during the 2010 Mw 7.1 Darfield (Canterbury) earthquake: Implications for fault rupture dynamics and seismic-hazard analysis. *Geology*, *40*(1), 55-58. https://doi.org/10.1130/g32528.1

Quigley, M., Van Dissen, R., Villamor, P., Litchfield, N., Barrell, D., Furlong, K., Stahl, T., Duffy, B., Bilderback, E., Noble, D., Townsend, D., Begg, J., Jongens, R., Ries, W., Claridge, J., Klahn, A., Mackenzie, H., Smith, A., Hornblow, S., . . . Pedley, K. (2010). Surface rupture of the Greendale Fault during the Darfield (Canterbury) earthquake, New Zealand: Initial findings. *Bulletin of the New Zealand Society for Earthquake Engineering*, *43*(4).

Rodgers, D. W., & Little, T. A. (2006). World's largest coseismic strike-slip offset: The 1855 rupture of the Wairarapa Fault, New Zealand, and implications for displacement/length scaling of continental earthquakes. *Journal of Geophysical Research: Solid Earth*, *111*(B12). https://doi.org/10.1029/2005jb004065

Schermer, E. R., Van Dissen, R., Berryman, K. R., Kelsey, H. M., & Cashman, S. M. (2004). Active faults, paleoseismology, and historical fault rupture in northern Wairarapa, North Island, New Zealand. *New Zealand Journal of Geology and Geophysics*, *47*(1), 101-122. https://doi.org/10.1080/00288306.2004.9515040

Seebeck, H., Van Dissen, R., Litchfield, N., Barnes, P. M., Nicol, A., Langridge, R., Barrell, D. J. A., Villamor, P., Ellis, S., Rattenbury, M., Bannister, S., Gerstenberger, M., Ghisetti, F., Sutherland, R., Hirschberg, H., Fraser, J., Nodder, S. D., Stirling, M., Humphrey, J., . . . Lee, J. (2023). The New Zealand Community Fault Model – version 1.0: an improved geological foundation for seismic hazard modelling. *New Zealand Journal of Geology and Geophysics*, *67*(2), 209-229. https://doi.org/10.1080/00288306.2023.2181362

Stirling, M., Fitzgerald, M., Shaw, B., & Ross, C. (2023). New Magnitude–Area Scaling Relations for the New Zealand National Seismic Hazard Model 2022. *Bulletin of the Seismological Society of America*, *114*(1), 137-149. https://doi.org/10.1785/0120230114

Stirling, M., McVerry, G., Gerstenberger, M., Litchfield, N., Van Dissen, R., Berryman, K., Barnes, P., Wallace, L., Villamor, P., Langridge, R., Lamarche, G., Nodder, S., Reyners, M., Bradley, B., Rhoades, D., Smith, W., Nicol, A., Pettinga, J., Clark, K., & Jacobs, K. (2012). National Seismic Hazard Model for New Zealand: 2010 Update. *Bulletin of the Seismological Society of America*, *102*(4), 1514-1542. https://doi.org/10.1785/0120110170

Teran, O. J., Fletcher, J. M., Oskin, M. E., Rockwell, T. K., Hudnut, K. W., Spelz, R. M., Akciz, S. O., Hernandez-Flores, A. P., & Morelan, A. E. (2015). Geologic and structural controls on rupture zone fabric: A field-based study of the 2010 Mw 7.2 El Mayor-Cucapah earthquake surface rupture. *Geosphere*, *11*(3), 899-920. https://doi.org/10.1130/ges01078.1

Tompkins, J. O. (1987). *Late Quaternary pollen stratigraphy, geology and soils of an area near Greytown.* Massey University.

Townsend, D., Begg, J., Villamor, P., & Lukovic, B. (2002). *Late Quaternary displacement of the Mokonui Fault, Wairarapa, New Zealand: A preliminary assessment of earthquake generating potential* (GNS Science client report, Issue 2024/58).

Van Dissen, R. J., & Berryman, K. R. (1996). Surface rupture earthquakes over the last ~1000 years in the Wellington region, New Zealand, and implications for ground shaking hazard. *Journal of Geophysical Research: Solid Earth*, *101*(B3), 5999-6019. https://doi.org/10.1029/95jb02391

Vella, P. (1963). Upper Pleistocene succession in the inland part of Wairarapa Valley, New Zealand. *Transactions of the Royal Society of New Zealand*, *2*(4), 63-78.

Villamor, P., Langridge, R. M., Ries, W., Carne, R., Wilson, K. J., Seebeck, H., & Cowan, L. (2008). *It's our fault, Wairarapa Fault slip rate investigations task: Completion report, is the Wairarapa Fault slip decreasing to the north?* (GNS Science consultancy report, Issue 2008/170).

Wallace, L. M., Barnes, P., Beavan, J., Van Dissen, R., Litchfield, N., Mountjoy, J., Langridge, R., Lamarche, G., & Pondard, N. (2012). The kinematics of a transition from subduction to strike-slip: An example from the central New Zealand plate boundary. *Journal of Geophysical Research: Solid Earth*, *117*(B2). https://doi.org/10.1029/2011jb008640

Wallace, L. M., Beavan, J., McCaffrey, R., & Darby, D. (2004). Subduction zone coupling and tectonic block rotations in the North Island, New Zealand. *Journal of Geophysical Research: Solid Earth*, *109*(B12). https://doi.org/10.1029/2004jb003241

Wang, N., & Grapes, R. (2008). Infrared-stimulated luminescence dating of late Quaternary aggradation surfaces and their deformation along an active fault, southern North Island of New Zealand. *Geomorphology*, *96*(1-2), 86-104. https://doi.org/10.1016/j.geomorph.2007.07.016

Warnes, P. N. (1992). Last interglacial and last glacial stage terraces on the eastern side of Wairarapa Valley between Waiohine and Waingawa Rivers. *Journal of the Royal Society of New Zealand*, *22*(4), 217-228.

Zachariesen, J., Villamor, P., Lee, J., Lukovic, B., & Begg, J. (2000). *Late Quaternary faulting of the Masterton and Carterton Faults, Wairarapa, New Zealand* (GNS Science client report, Issue 2000/71).

Zielke, O., & Arrowsmith, R. (2012). LaDiCaoz and LiDARimager—MATLAB GUIs for LiDAR data handling and lateral displacement measurement. *Geosphere*, *8*(1), 206-221. https://doi.org/10.1130/ges00686.1

Figure Captions

Figure 1 – Tectonic overview of A) the Aotearoa - New Zealand plate boundary and B) the southern North Island. AF is the Alpine Fault and HT is the Hikurangi Trough. Onshore active faults are shown in red and are from the 1:250,000 scale New Zealand Active Faults Database (Langridge et al. 2016) and includes updated active fault mapping presented in this paper. Offshore faults are shown in dark grey (Barnes et al., 2010; Nodder et al., 2007). The Wairarapa Valley is shaded in yellow. The Wairarapa Region is indicated by the bold black outline and district boundaries (South Wairarapa, Carterton, Masterton) are indicated by the white lines.

Figure 2 - Geological and faulting overview of the northern Wairarapa Valley. Generalised geological units are from the 1:250,000k Quarter Million Map (QMAP) (Begg & Johnston, 2000; Lee & Begg, 2002). Active fault mapping is coloured by dominant slip sense and includes the newly identified Woodside (WoF), Carters Line (CLF), Pāpāwai (PF), Ruamahanga (RF), Te Hau (THF), and Mangaterere (MGF) faults, as well as updates to the Wellington (WeF), Wairarapa (WaiF), Mokonui (MoF), Masterton (MaF), Carterton (CF) and Eastern Carterton (ECF) faults.

Figure 3 - Active faults mapped in the Wairarapa Region prior to (A) and after (B) the lidar mapping described in this work. Previous mapping shown in (A) is from the 1:250,000 scale New Zealand Active Faults Database (NZAFD; Langridge et al. 2016; Morgenstern et al. 2024). Faults shown in (B) includes the updated mapped active fault traces, which are coloured maroon if they had previously been identified and in red if they were newly identified as part of this work. Newly identified faults are as follows:

Wharekauhau East (WEF), Woodside (WoF), Pāpāwai (PF), Carters Line (CLF), Mangaterere (MgF), Ruamahanga (RF), and Te Hau (THF) faults. One fault was removed upon re-evaluation of fault mapping, the Ngāpotiki Fault (NF). The Battery Hill Fault (BHF) is also indicatedOne fault was removed upon re-evaluation of fault mapping, the Ngāpotiki Fault (NF) and the Battery Hill Fault (BHF) is also indicated. The blue shaded polygon in (B) encompasses the areas within the Coastal Range where mapping was not focused. All updated active fault mapping is included in can be found on the NZAFD (https://data.gns.cri.nz/af/).

Figure 4 - Revised terrace mapping in the northern Wairarapa Valley. The Ruamahanga, Carters Line), Woodside), and Pāpāwai faults are indicated by the coloured lines. All other faults are shown in dark grey. Circled letters indicate the main sites where terrace mapping changed and are discussed in the text.

Figure 5 – The four newly mapped active faults in the northern Wairarapa Valley that are described in the text. A) Location and overview of the four faults discussed in the text. The Ruamahanga Fault is shown in blue, the Woodside Fault in yellow, the Carters Line Fault in green and the Pāpāwai Fault in purple. B – E) Detailed mapping for each fault. (a) and (b) in panel D are grouped traces of the Carters Line Fault discussed in the text. Note the orientation of the north arrow and colour scale changes between panels.

Figure 6 – Examples of mapping of the Mokonui Fault from lidar data. A) Overview of the Mokonui Fault (red) and the northern Wairarapa Fault (dark grey). B, D, and F) Lidar maps demonstrate kinematic styles of the Mokonui Fault. C, E, G) Annotated versions of B, D, and F) with the Mokonui Fault shown in red.

Figure 7 – Examples of the method used to measure maximum fault scarp gradients. A) Mokonui Fault, B) Wairarapa Fault, and C) Ruamahanga Fault. Insets show the fault

sampled (red line), the yellow line is the orthogonal profile along which scarp gradient was measured. The dark blue line is the profile extracted from the lidar data, and the part of this line shown in red indicates the 2 m horizontal interval portion with the highest (steepest) gradient. Note the y-axes for each profile are scaled differently.

Figure 8- Summary of slip rates calculated for the A) Ruamahanga, B) Woodside, C) Carters Line, and D) Pāpāwai faults Ruamahanga (A) Pāpāwai (B), Woodside (C), and Carters Line (D) faults. Green points indicate locations where a vertical slip rate was measured, and magenta points indicate where a horizontal slip rate was measured. Black rectangles delineate where an average slip rate was calculated from individual slip rate measurements and summed across multiple strands.

Figure 9 – Normalised fault scarp gradient data for faults in the northern Wairarapa Valley. Warmer colours indicate steeper gradients. Faults are shown as grey lines and are as follows: Wairarapa Fault (WaiF), Mokonui Fault (MoF), Ruamahanga Fault (RF), Masterton Fault (MaF), Carterton Fault (CF), Carters Line Fault (CLF), Pāpāwai Fault (PF), Woodside Fault (WoF).

Figure 10 – A) Version 1.0 of the NZ CFM (Seebeck et al. 2024). B) Suggested revision of the CFM in the Wairarapa following the results of the active fault mapping presented here. The faults are as follows: MgoF – Mangaoranga Fault, DRF – Dry River Fault, THF – Te Hau Fault, MoF – Mokonui Fault, MgtF – Mangatoro Fault, MaF – Masterton Fault, RF – Ruamahanga Fault, CF – Carterton Fault, WeF – Wellington Fault, PF – Pāpāwai Fault, Wo-CLF – Woodside-Carters Line Fault, KF – Kaumingi Fault, MotF – Motumatai Fault, WaiF – Wairarapa Fault, FPF – Flatpoint Fault, TMF – Te Maire Fault, MarF – Martinborough Fault, HF – Huangarua Fault, OF – Otaraia Fault, DF – Dry River Fault,

PiF – Pirinoa Fault, BHF – Battery Hill Fault NF - Ngāpotiki, EWT – Eastern Wharekauhau Thrust, and WT – Wharekauhau Thrust. A shapefile with the suggested update to the NZ CFM is included in the Supplementary Materials.